3D Cell Aggregates Amplify Diffusion Signals

Hamidreza Arjmandi[1], Kajsa P Kanebratt[2], Liisa Vilén[2], Peter Gennemark[2,3], Adam Noel[1*],

1 School of Engineering, University of Warwick, Coventry, UK.
2 Drug Metabolism and Pharmacokinetics, Research and Early Development, Cardiovascular, Renal and Metabolism (CVRM), AstraZeneca, Gothenburg, Sweden.
3 Department of Biomedical Engineering, Linköping University, Sweden.

☯Hamidreza Arjmandi derived the theory, implemented the simulator, co-conceived the experiment, analyzed the results, wrote the manuscript excluding Experimental Methods. Kajsa P Kanebratt conducted experiment and wrote the Experimental Methods. All authors co-conceived the idea of the manuscript and the experiment, discussed the theoretical and experimental results, and reviewed the manuscript.
* adam.noel@warwick.ac.uk

Abstract

Biophysical models can predict the behavior of cell cultures including 3D cell aggregates (3DCAs), thereby reducing the need for costly and time-consuming experiments. Specifically, mass transfer models enable studying the transport of nutrients, oxygen, signaling molecules, and drugs in 3DCA. These models require the defining of boundary conditions (BC) between the 3DCA and surrounding medium. However, accurately modeling the BC that relates the inner and outer boundary concentrations at the border between the 3DCA and the medium remains a challenge that this paper addresses using both theoretical and experimental methods. The provided biophysical analysis indicates that the concentration of molecules inside boundary is higher than that at the outer boundary, revealing an amplification factor that is confirmed by a particle-based simulator (PBS). Due to the amplification factor, the PBS confirms that when a 3DCA with a low concentration of target molecules is introduced to a culture medium with a higher concentration, the molecule concentration in the medium rapidly decreases. The theoretical model and PBS simulations were used to design a pilot experiment with liver spheroids as the 3DCA and glucose as the target molecule. Experimental results agree with the proposed theory and derived properties.

Author summary

The primary objective of our research was to enable the development of reliable biophysical models for three-dimensional cell aggregates (3DCAs). To achieve this goal, we employed a combination of theoretical and experimental methods to derive and characterize the amplification boundary condition (BC), which represents the relation of inner and outer boundary concentrations at the border between a 3DCA and its surrounding medium. By understanding the amplificaiton BC, we can better comprehend the transport and diffusion processes that occur within 3DCAs.

The significance of our research lies in its potential to advance the understanding of 3DCAs and their underlying biophysical processes. This knowledge is crucial for a

wide range of applications, including drug design and analysis of drug dosages within tissues. This factor may provide insight into the mechanisms behind tumor development and morphogenesis. In particular, the packed structure of cancer tumors enables them to receive and trap a higher concentration of nutrients and oxygen molecules based on the amplification factor. Thus, this study could contribute to the development of novel approaches to manage and treat cancerous tissues.

Introduction

The term *3D cell aggregate (3DCA)* refers to any type of *in vitro* model in which cells are grown in three dimensions, as opposed to the traditional 2D monolayer culture. Organoids, spheroids, and tumoroids are all examples of 3DCA models, each with unique characteristics and applications. 3DCAs have received great attention and popularity in recent years due to their ability to better mimic the complex microenvironments and cell-cell interactions within *in vivo* tissues, in comparison to traditional 2D cell cultures [1]. 3DCAs can be composed of several different cell types, e.g., hepatocytes and stellate cells to form liver spheroids [2]. They can be used to model organ development and disease progression and they have a wide range of applications in basic biological research, drug discovery, and regenerative medicine [3]. Organ-on-chips (OoCs) as bioengineered microdevices use the 3D nature and arrangement of 3DCAs to recapitulate key functional properties of organs and tissues [4].

Biophysical models are important mathematical and computational tools to describe physical and chemical properties of biological processes and systems including 3DCAs [1]. They integrate biological data with mathematical equations or algorithms to simulate the behavior of the biological system [5–7]. These models could be beneficial to 3DCA studies in several ways. Biophysical models can predict the behavior of 3DCAs under various conditions such as applied stimuli. Thus, they can be used to optimize the 3DCA conditions and to reduce the need for expensive and time-consuming experimental assays by predicting the outcomes under different experimental conditions. Also, we can use these models to integrate data from multiple scales [8], ranging from the molecular and cellular levels to the tissue level, to provide a comprehensive understanding of the behavior of 3DCAs. Furthermore, biophysical models may reveal new phenomena that might not be observable through experiments alone.

Mass transfer models are a crucial category of biophysical models that can enable researchers to study the transport of essential molecules, including nutrients, oxygen, signaling molecules, and drugs in 3DCAs. Specifically, the transfer of diffusible nutrients, like oxygen, plays a vital role in regulating fundamental cellular processes such as cell migration, death, and progression through the cell cycle [9, 10]. 3DCAs rely on a culture medium that fills the extracellular space within the cell aggregate and creates a continuous fluidic environment where molecules are transferred through two transport mechanisms, diffusion and flow, which can both contribute to the mass transfer model. When there is slow flow, or in avascular 3DCAs where there is no vascular system to deliver nutrients and oxygen, the diffusion mechanism dominates in the mass transfer model. Diffusion of molecules in an environment is described by Fick's laws of diffusion which are defined by partial differential equations that describe the change in concentration of diffusing molecules with respect to time and space [11].

The diffusion of molecules within the medium outside and inside a 3DCA should be modeled differently to account for the varying physical and chemical properties of the porous structure of the 3DCA. A simplified model for medium diffusion inside a 3DCA is to treat the 3DCA as a porous medium with a corresponding diffusion coefficient

that scales down the diffusion coefficient in the free culture medium. To model diffusion of molecules within the medium inside and outside the 3DCA, one can consider two diffusion environments with different diffusion coefficients. The concentration of diffusing molecules is characterized through two partial differential equations. These two equations are connected by defining two boundary conditions (BCs) at the 3DCA border that relate the concentration of molecules inside and outside of the boundary. The first BC is the flow continuity condition, which is applied at the border to ensure equal mass flux across the boundary. The second BC is characterized by the concentration ratio inside and outside of the 3DCA border [11]. This BC, referred to as the *amplification BC* throughout the rest of this paper, accounts for the influence of the 3DCA on the diffusive transport of molecules and has a significant impact on the accuracy of the diffusion model.

Despite its importance, the amplification BC has not been comprehensively characterized in the literature, and different types of models have been proposed by various authors. Some works define the amplification BC as a unitary ratio, implying that the concentration is the same inside and outside the 3DCA border [12–15]. Astrauskas et al. (2019) presented a reaction-diffusion equation model for the analysis of dye penetration into cellular spheroids in which the unitary ratio is employed to model the boundary condition [12]. Leedale et al. (2020) proposed a diffusion model for drug transport and metabolism that is developed in a multiscale spheroid framework, accounting for microscale processes where the concentration at the boundary is simply assumed to be equal to the outside concentration [13]. Bull et al. (2021) developed a hybrid, off-lattice agent-based model for oxygen-limited spheroid growth [14]. The concentration at the spheroid boundary is assumed to be maintained at the constant oxygen concentration in the culture medium, i.e., the unitary ratio is implied. As part of his thesis, Rousset (2022) studied the molecule diffusion into and consumption by a spheroid where the unitary ratio is used to model the boundary condition [15].

In other works, a porosity ratio is assumed for the 3DCA BC, where the concentration inside the boundary is expressed as the concentration outside the boundary multiplied by the porosity coefficient. Graff et al. (2003) developed a mathematical model to provide an improved understanding of the quantitative interplay among the rate processes of diffusion, binding, degradation, and plasma clearance in antibody penetration of tumor spheroids [16]. The authors considered the concentration at the spheroid boundary to be equal to the concentration outside multiplied by the spheroid porosity. In other words, they assumed that the molecule concentration at the *extracellular space* boundary is equal to the concentration outside the spheroid. A similar boundary condition has been considered by Goodman et al. (2008), where the authors developed a mathematical model of nanoparticle penetration into multicellular spheroids that accounts for radially-dependent changes in tumor architecture [17].

Furthermore, some authors have modeled the diffusion process only inside the 3DCA where they consider a constant concentration insider the boundary but do not relate it to the concentration outside the boundary [18, 19]. Grimes et al. (2014) employed an oxygen diffusion model in three-dimensional tumor spheroids to present a method for estimating rates of oxygen consumption from spheroids [18]. The concentration at the boundary of the tumor is assumed to be constant and unrelated to the concentration in the surrounding media. In other words, a model with one diffusion environment is assumed where the concentration inside the border is fixed. Klowss et al. (2022) developed a stochastic model that provides quantitative information about nutrient availability within a spheroid [19]. Similar to Grimes et al. (2014) [18], Klowss et al. (2022) only modeled the diffusion inside the spheroid given

that the nutrient concentration at the boundary is constant and equal to some maximum far-field concentration.

These diverse approaches demonstrate the existing inconsistency and ongoing challenge to accurately model the mass transport process in 3DCAs and motivates us to more precisely derive and characterize the amplification BC between 3DCAs and the surrounding media using theoretical and experimental methods. We use an effective diffusion model to describe the porous structure of 3DCAs and determine the corresponding diffusion coefficient and concentration. To quantify the amplification BC, we analytically demonstrate that the concentration of molecules inside the boundary is amplified relative to the concentration at the outer boundary by a factor that is greater than or equal to one, which we refer to as the *amplification factor*.

To provide an intuitive explanation for the boundary amplification factor, let us consider a 3DCA culture inside a microfluidic chip compartment or well that is exposed to a medium containing a known concentration of molecules. Due to the concentration gradient, molecules begin to enter the cell culture. However, the smaller diffusion coefficient within the 3DCA causes molecules that are freely diffusing in the well to become (relatively) trapped and absorbed within the 3DCA extracellular space. As a result, we expect that molecules accumulate inside boundary of the 3DCA, leading to a higher concentration than that outside the boundary. We want to emphasize that the amplification factor is a biophysical property related to diffusion, distinct from the (bio)chemical concepts of partition coefficient and solubility [20]. The partition coefficient is a measure of the ratio of concentrations of a compound in a mixture of two immiscible solvents at equilibrium, and typically serves to quantify the degree to which a chemical substance exhibits hydrophilicity ("water-loving") or hydrophobicity ("water-fearing"). Solubility measures the ability of substances to interact and form solutions.

We have provided a particle-based simulator (PBS) in which the Brownian motion of molecules is tracked and updated independently on both sides of the boundary, and passage across the boundary is treated accordingly. The PBS confirms the analytical result and reveals that a non-unitary amplification factor could lead to a noticeable impact on the molecule concentration in the medium when we add low-porosity cell cultures to the medium. When a 3DCA containing a lower concentration of target molecules is placed in a medium with a higher concentration of these molecules, our PBS reveals a rapid decrease in the concentration of the molecules in the culture medium. This rapid behaviour as a result of the amplification factor is a possible explanation for the observed initial offset in glucose concentration reported by Casas et al. (2022) [21] and similar 3DCA experiments. We leverage our proposed PBS to design a pilot experiment that could provide a mechanistic explanation to the initial offset due to the amplification factor. Furthermore, this experimental method can be used to characterize the amplification factor.

For our experimental case study, we used liver spheroids as our 3DCAs and glucose as our target molecule. Prior to introducing the liver spheroids to a medium with a high glucose concentration of 11 mM, they were kept in two pre-culture media of volume 100 and 75 μL with a glucose concentration of 2.8 mM. Our experimental findings show a reduction in glucose concentration within the medium ($p = 0.008$ for 100 μL medium and $p = 0.06$ for 75 μL) over a very short time of 10 minutes. Additionally, our PBS results closely align with the experimental results, particularly for a media volume of 100 μL.

The remainder of this paper is organized as follows. We present the theoretical modeling including the mathematical proof. Then, we introduce the experimental methods employed, beginning with our approach to revealing the rapid drop in medium concentration, followed by the proposed PBS to confirm our theoretical

results and the designed experiment. Finally, the results are discussed and the conclusions are presented.

Theoretical Methods

Modeling of Diffusion BCs at the Border of 3DCA

A 3DCA with volume V_s formed by N_c cells including $N_c^1, \cdots, N_c^Q$ of Q different types is considered. The culture's interior space is comprised of the cells and the extracellular space between the cells. Given that the volume of cell type i is V_c^i, the total volume of the cells and the extracellular space inside the 3DCA are given by $\sum_{i=1}^{Q} V_c^i N_c^i$ and $V_s - \sum_{i=1}^{Q} V_c^i N_c^i$, respectively.

We model the 3DCA structure as a porous medium with volume V_s whose porosity, ϵ, is defined as the ratio of the extracellular space to the whole 3DCA volume, i.e.,

$$\epsilon = 1 - \frac{\sum_{i=1}^{Q} V_c^i N_c^i}{V_s}. \tag{1}$$

We assume that the cell culture is in a fluid medium that surrounds it and fills its extracellular space. The diffusive signaling molecules of type A in the medium can diffuse into the extracellular space of the cell culture. In order to analyze the diffusion effect exclusively, we assume that there is no chemical reaction or binding occurring between the cells and target molecules within the cell culture structure. This assumption reasonably holds over a sufficiently short timescale when the culture is first exposed to the medium and the diffusion effect dominates. It is especially applicable when the rate of molecule binding and consumption is much slower than diffusion, such as in the case of glucose uptake by liver cells which is known to be much slower (i.e., hours) than the diffusion process in minutes [2].

Ideally, the porous culture structure acts as a net, enabling molecules outside the cell culture to pass through its border with a probability that depends on the surface porosity of the culture. This surface porosity can be estimated based on the geometric projection of volume porosity (ϵ) in 3D onto 2D using $\epsilon_s = \epsilon^{\frac{2}{3}}$. Inside the 3DCA, the molecules diffuse via the curved paths of the extracellular space among the cells, which leads to a shorter net molecule displacement within a given time interval. Thus, macroscopic diffusion within the cell culture effectively differs from the diffusion within the free fluid outside it. Since the molecules traverse a shorter net path within the cell culture, the effective diffusion coefficient is smaller than the diffusion coefficient in the free fluid medium and molecules are more likely to be observed and sensed by the culture's cells (see Fig. 1).

Fig 1. (a) The curved path of molecule trajectories within a spheroid leads to an effective diffusion coefficient smaller than the diffusion coefficient of the free medium, i.e., $D_{\text{diff}} < D$. (b) Boundary between media outside of 3DCA and the effective diffusion model for 3DCA which is a free medium diffusion environment with D_{diff}. The net (dashed line) at the boundary models the surface porosity and corresponding molecule reflection. The concentration and number of molecules at both sides are shown for a small volume very close to the boundary. (c) Boundary between media outside and inside the 3DCA that includes both the cells and extracellular space.

We assume that the extracellular space within the 3DCA is homogenized to model an effective diffusion environment throughout the entire culture volume. Given the diffusion coefficient D for molecules A in the free fluid, the effective diffusion coefficient

within the entire cell culture volume (homogenized environment) is given by [24]

$$D_{\text{eff}} = \frac{\epsilon}{\tau} D, \tag{2}$$

where τ is the tortuosity, a measure of the transport properties of the porous medium, and is modeled as a function of cell culture porosity as $\tau = \frac{1}{\sqrt{\epsilon}}$ [23].

These two diffusion environments inside and outside the 3DCA are connected by defining two boundary conditions (BCs) at the border of the 3DCA. The first BC is the following flow continuity condition, which is applied at the border to ensure equal mass flux across the boundary:

$$D_{\text{eff}} \nabla c_s(\bar{r}, t) \cdot \hat{n} = D \nabla c_o(\bar{r}, t) \cdot \hat{n}, \qquad \bar{r} \in \partial\Omega, \tag{3}$$

where $\partial\Omega$ denotes the boundary region of the cell culture, $\hat{n}$ is the normal vector at the border point $\bar{r}$, c_o is the concentration of molecules outside the cell culture, and c_s is the concentration of molecules inside the equivalent diffusion model of the cell culture, i.e., a free diffusion environment of volume V_s with diffusion coefficient D_{eff}. Thus, the concentration inside the extracellular space within the cell culture is given by c_s/ϵ. For the two diffusion environments, the second BC is characterized by the concentration ratio inside and outside of the 3DCA border as [11]

$$c_s(\bar{r}, t) = k c_o(\bar{r}, t), \qquad \bar{r} \in \partial\Omega, \tag{4}$$

where k has not been derived and is suggested to be determined experimentally [11]. This is a common BC model used for the border of a 3DCA with surrounding media. Despite its importance, this second BC for a 3DCA inside media has not been comprehensively or consistently characterized in the literature. However, the amplification factor should be derived as a function of medium porosity.

We refer to the BC (4) and k as the *amplification BC* and *amplification factor*, respectively. The amplification BC accounts for the influence of the 3DCA on the diffusive transport of molecules and has a significant impact on the accuracy of the diffusion model. We previously used a PBS for a system with a spheroid inside an unbounded environment as two ideal diffusion environments with diffusion coefficients D and D_{eff} and, without any net barrier, the simulation results suggested $k = \sqrt{\frac{D}{D_{\text{eff}}}}$ [25]. Here, we theoretically prove that $k = \sqrt{\frac{D}{D_{\text{eff}}}}$ generally characterizes the amplification BC for a 3DCA inside a medium modeled as two diffusion environments separated by a border with porosity of ϵ_s. Since the boundary is assumed to be ideal, a particle that passes through the border will follow its arrival direction and not change direction. As a result, we can assume a one-dimensional diffusion environment for the proof, without any loss of generality.

Proposition 1: For two ideal diffusion environments with diffusion coefficients D and D_{eff} separated by a surface with porosity ϵ_s and concentration functions $c_o(x), x \in [-\infty, 0]$ and $c_s(x), x \in [0, \infty]$, the amplification factor is equal to

$$k = \sqrt{\frac{D}{D_{\text{eff}}}}. \tag{5}$$

The proof is provided in the Appendix S1.

Thus, for $k \neq 1$, a concentration discontinuity (i.e., jump) occurs at the boundary. Therefore, the concentration is amplified by factor k when passing through the cell culture boundary. In the scenario involving two general diffusion environments, it is possible to encounter a situation where $k < 1$, which is inconsistent with the concept

of an *amplification* factor. We employ the term "amplification" to emphasize the elevated concentration observed within a 3DCA.

We note that kc_o is the inner boundary concentration within the *equivalent free diffusion* environment with diffusion coefficient D_{eff}. Therefore, the concentration within the extracellular space inside of the cell culture boundary would be $\frac{kc_o}{\epsilon}$.

Experimental Methods

In this section, we reveal and analyze an emergent property of 3DCAs caused by the amplification factor acting at the culture boundary. This property can influence the outcomes and interpretations of experiments involving 3DCAs. To measure and characterize the amplification factor, we utilize this property to design an *in vitro* experiment in which the liver spheroids are exposed to a fluid medium with glucose molecules. We use a PBS that accurately emulates the experimental activity and enables us to gain further insights into the relevant parameters required to carry out the experiment.

Rapid concentration reduction in culture medium

To provide an intuitive explanation for the boundary amplification factor, let us consider a 3DCA culture inside a microfluidic chip compartment or experimental well that is exposed to a medium containing a known concentration of molecules. Due to the concentration gradient, molecules begin to enter the cell culture. However, the smaller diffusion coefficient within the 3DCA causes molecules that are freely diffusing in the well to become (relatively) trapped and absorbed within the 3DCA extracellular space. In other words, due to the small effective diffusion coefficient inside the cell culture, it takes a longer time for molecules to exit.

As a result, we expect that molecules accumulate within the cell culture, thus reducing the concentration of the molecules in the medium, provided that there are no reactions between cells and molecules that occur faster than the transient diffusion behavior. This phenomenon is a consequence of the amplification factor that comes from the smaller effective diffusion coefficient inside the cell culture. Obviously, the concentration reduction would be more significant for larger cell culture volumes and higher amplification factors. To provide a preliminary estimate of the concentration change, let us make some simplifying assumptions and perform some quick insightful calculations.

Let us consider a well that is filled with a medium of volume V_m and a molecule concentration of C_m. Next, we introduce N_s 3DCAs, such as spheroids, to the medium. Prior to this, the cell cultures were maintained in a pre-culture medium with a concentration $C_p < C_m$. Initially, the molecule concentration in the spheroids is expected to be $C_s < kC_p$, assuming no reaction or consumption of the molecules, with a homogeneous distribution of molecules within the spheroids.

We can assume that each spheroid contains C_sV_s molecules at the time of being added to the well. After a brief period of time, numerous molecules are expected to have diffused into the spheroids due to the concentration gradient. We can further assume that molecule reactions with the cells are significantly slower than the diffusion rate within the spheroids. As a result, no molecule is lost due to reaction during the transient period when there is net diffusion of molecules into the spheroid.

Under these conditions, the molecule concentration within the spheroid will increase and eventually reach a local time equilibrium C'_s. At the same time, the molecule concentration in the medium decreases to a constant average level denoted by C'_m. By local time equilibrium, we mean that the concentration throughout the

whole spheroid(s) will be uniform for that short time. Given the boundary condition in (4), the concentration inside the spheroid will be $C'_s = kC'_m$. To obtain C'_s and C'_m, we consider the molecule conservation in this closed system. The total number of molecules at time $t = 0$ was $C_m V_m + N_s C_s V_s$, which is equal to the number of molecules shortly thereafter at the local time equilibrium. Therefore, we have

$$C'_m V_m + N_s C'_s V_s = C_m V_m + N_s C_s V_s. \tag{6}$$

By applying $C'_s = kC'_m$ and the bound $C_s < kC_p$, we obtain

$$C'_m < \frac{C_m V_m + N_s k C_p V_s}{V_m + k N_s V_s}. \tag{7}$$

Equivalently, the concentration reduction in the medium is obtained as

$$C_m - C'_m \geq \frac{(C_m - C_p) k N_s V_s}{V_m + k N_s V_s}. \tag{8}$$

From (8), a higher k value could further reduce the medium concentration inside the well while increasing the concentration inside the cell culture. However, this analysis is valid at equilibrium, and the exact time-point when this equilibrium occurs is unknown to us. On the other hand, if we wait too long to measure, then the biochemical reactions in the cell pathways may significantly affect the molecule concentration inside the spheroids. In particular, for our pilot experiment, the liver cells take up glucose molecules. To better clarify these points, we use a PBS that is able to track transient molecule concentration and we use liver cells taking up glucose molecules in our experiment, which is known to be much slower (i.e., hours) than the diffusion process [2].

Particle-based simulator

We use liver spheroids created by differentiated HepaRG cells and human hepatic stellate cells following the method described by Bauer et al. (2017) [2] for our simulations and pilot experiment. Supplementary Figure S1 displays images of six spheroids that were formed using this method, shown at two different scales. Each image displays the maximum projected area of a spheroid in 2D. To determine the spheroid's area within the image, the software tool ImageJ [27] was utilized, and the radius of a circle with equivalent area is used as the spheroid's radius. The average spheroid radius across these 6 samples was found to be $R_s = 226$ μm.

The total number of cells in each spheroid is assumed to be $N_c = 25000$ including 24000 HepaRG cells and 1000 human hepatic stellate cells, as reported by Bauer et al. (2017) [2]. The diameter of differentiated HepaRG cells has been reported as 17 μm [26]. The volume of HepaRG cells is calculated to be approximately 1.7×10^{-15} m^3, assuming a spherical or cubic shape with this diameter, as a mean reference. Since the number of hepatic stellate cells in the spheroid is negligible in comparison to HepaRG cells, we can make a rough assumption that the volume of a hepatic stellate cell is approximately the same as a HepaRG cell, as this simplification does not significantly impact our calculations. Thereby, using $N_c = 25000$, we obtain $\epsilon = 0.1$ and correspondingly $k = 4.49$.

We considered a flat-bottomed well with a radius of $R_w = 3.2$ mm and a height of 6.2 mm for our *in vitro* experiment. We chose to use medium volumes of $V_m = \{100, 75\}$ μL. To demonstrate the amplification factor and resulting concentration reduction in the culture medium, we chose a high glucose concentration of 11.12 mM (hyperglycemia) [2] in the incubation medium and a low glucose

concentration of 2.8 mM in the pre-culture medium to keep the spheroids alive. The large difference between these two concentrations helps to highlight the effect of the amplification factor.

To simulate the concentrations of 11.12 mM and 2.8 mM glucose in the culture and pre-culture media, respectively, with particle-based simulations, we would require a very large number of molecules and that is not computationally feasible. However, since the molecules move independently in the PBS, we do not need to use the exact number of molecules corresponding to these concentrations. Instead, we randomly placed $N_m = C_m V_m = 10^6$ molecules within the medium space and $C_s V_s = k C_p V_s$ molecules within each spheroid where $C_p = \frac{N_m}{V_m} \times \frac{2.8}{11.12}$, which leads to the same ratio of 11.12:2.8 between the medium and pre-culture medium. We normalized the concentration values by the initial concentration inside the medium, which was set to 1, in order to demonstrate the results.

In the PBS, time is divided into time steps of $\Delta t = 0.1$ s. In each time step, the molecule locations are updated following random Brownian motion. The molecules move independently in the 3-dimensional space, either in the medium or within the spheroids where the displacement of a molecule in Δt s is modeled using Gaussian random variables both with zero mean and variances $2D\Delta t$ and $2D_{\text{eff}}\Delta t$, respectively, along each dimension (Cartesian coordinates), where $D = 10^{-9}$ and $D_{\text{eff}} = 4.2 \times 10^{-11}$ m^2/s obtained from (2).

In reality, the movement of molecules outside the spheroid may be affected by the porous spheroid surface. Molecules may pass through the extracellular spaces of the surface or reflect back if they hit other parts of the surface. For the simulation, the surface porosity of the spheroid is represented by the probability ϵ_s, which is the likelihood that a hitting molecule will enter the surface. For molecules inside the spheroid, we assume an equivalent diffusion environment with an effective diffusion coefficient D_{eff}.

We note that in this simplified environment model, the molecules can move freely inside the spheroid, and the porous structure effect is taken into account by using the effective diffusion coefficient. However, like the molecules outside, the molecules diffusing inside the equivalent environment may collide with the spheroid wall and exit with a probability of ϵ_s. We note that the opening sites over the boundary enables the passage of molecules in both directions, i.e., from the outside to the inside of the spheroid and vice versa. Consequently, we assume an equal probability of ϵ_s for movement in either direction.

Considering the mismatch between the diffusion coefficients, we need to update the displacement vector of a molecule that crosses the spheroid boundary. For example, consider that a molecule in the medium outside a spheroid and its displacement vector during Δt s is $(\Delta x, \Delta y, \Delta z)$ with a length of d_T that would move the molecule into the spheroid. This vector has two parts: one part of length d_o outside the spheroid and one part of length d_i inside the spheroid. Then, the vector length for the inside part needs to be scaled by the factor $\sqrt{\frac{D}{D_{\text{eff}}}}$. As a result, the displacement vector is updated as follows

$$\frac{d_o + \left(\sqrt{\frac{D}{D_{\text{eff}}}} d_i\right)}{d_T} (\Delta x, \Delta y, \Delta z). \tag{9}$$

Similarly, if a molecule moves from inside to outside of the spheroid, then we need to update displacement vector outside according to

$$\frac{d_i + \left(\sqrt{\frac{D_{\text{eff}}}{D}} d_o\right)}{d_T} (\Delta x, \Delta y, \Delta z). \tag{10}$$

We also consider the cases where molecules diffusing within the well environment may hit the well walls or the top surface of the medium. In all these cases, the molecules are reflected back inside the well.

Figure 2(a) presents the normalized glucose concentration (NGC) both inside and outside the spheroid for medium volumes of 75 and 100 μL. The arrows indicate the ratio of NGC inside the spheroid to NGC outside, which is found to be approximately $k = \sqrt{\frac{D}{D_{\text{eff}}}}$, as derived in (5). In Fig. 2(b), we show a higher resolution view of NGC in the medium for both volumes.

Fig 2. (a) Normalized glucose concentration (NGC) inside and outside the spheroid as a function of time for both medium volumes of 75 and 100 μL obtained by PBS. NGC inside the spheroids is the average over all 40 spheroids in the well. The ratio of NGC inside the spheroid to NGC outside is approximately 4.5. (b) A higher resolution view of NGCs in the medium for both volumes provided in Fig. 2(a). (c) The predicted time-averaged GC for medium volumes of 75 and 100 μL after a period of 10 minutes based on the results in Fig. 2(b).

The concentration dynamic in the first 10 minutes (which is significantly shorter than the duration of the glucose uptake process by the spheroids) suggests that measuring the time-averaged NGC provides a good estimate of the NGC reduction due to the spheroids. Fig. 2(c) shows that the predicted time-averaged GC for medium volumes of 75 and 100 μL over a period of 10 minutes is found to be 10.37 and 10.58, respectively, corresponding to a 5.7 and 3.8 percent GC reduction in the media, respectively. Therefore, in the *in vitro* experiment we took samples at 1, 5, and 10 minutes (min) after addition of spheroids to high-glucose medium to estimate the time-averaged NGC during the first 10 min, as chemical reactions may have a significant impact at longer timescales. We calculated the number of replicates required to achieve a power of 80 percent to distinguish these GC reductions from 11.12 mM, considering a variance of 0.15 for measurements and a significance level of 0.1. The required number of replicates was 3 and 4 for the two cases, respectively, to achieve a power of 80 percent. However, we conducted 8 replicates for each case to achieve a higher level of confidence.

Liver Spheroid Formation and Glucose Assay

Formation of liver spheroids is based on the method published by Bauer et al. (2017) [2]. Differentiated HepaRGs (Lot HPR116239) were obtained from Biopredic International (Rennes, France). Primary human hepatic stellate cells (HHSteC), lot PFP, were purchased from BioIVT (Brussels, Belgium).

The differentiated HepaRGs were thawed and seeded confluently three days before spheroid formation. Standard HepaRG culture medium consisted of Williams Medium E without glucose (PAN-Biotech, Aidenbach, Germany) supplemented with 10% foetal bovine serum (Gibco, ThermoFisher Scientific, Waltham, MA, USA), 11.12 mM glucose (SigmaAldrich, St. Louis, MO, USA), 5 μg/mL human insulin (Gibco), 2 mM L-glutamine (Corning), 50 μM hydrocortisone hemisuccinate (SigmaAldrich), 50 μg/mL gentamycin sulfate (Gibco) and 0.25 μg/mL Amphotericin B (Gibco). On the following day, the medium was renewed with HepaRG medium containing 2% dimethyl sulfoxide. The cells were maintained in this medium for two days until spheroid formation. HHSteC were expanded in Stellate Cell Medium, provided by ScienCell (Carlsbad, CA, USA). Cells were used in passage 3. Pre-culture was started two days before spheroid formation.

Human liver spheroids were formed combining differentiated HepaRG cells and

HHSteC using 384-well spheroid microplates (Corning, Lowell, MA, USA) in HepaRG medium. Briefly, 50 μL containing 24,000 hepatocytes and 1,000 HHSteC was pipetted into each well of the spheroid plate. The plate was centrifuged for 1 min at 300 xg and incubated at 37 °C and 5% CO2. Two days after seeding, 20 μL medium was removed and 50 μL fresh medium was added to the spheroids and five days after seeding 50% medium was renewed.

Six days after seeding, 40 spheroids were pooled into a 24-well ultra low attachement plate (Corning). The spheroids were washed once with 500 μL HepaRG medium with 2.8 mM glucose and 1 nM insulin. After the wash, 800 μL of this medium was added and spheroids were incubated for 2 h. Spheroids were then transferred to a 96-well flat bottom ultra low attachment plate (Corning) and medium was changed to 75 or 100 μL (8 replicates per volume) HepaRG medium with 11.12 mM glucose and 870 nM insulin. Medium samples were taken after 1, 5, and 10 min and HepaRG medium with 11.12 mM glucose and 870 nM insulin was sampled as 0 min control. For samples where starting volume was 100 μL, a medium sample was also taken after 4 h. For samples with starting volume of 75 μL, all medium was removed after 10 min sampling and 100 μL new medium was added. From these incubations, the medium was sampled after 19 h. Fig. 3 represents the schematic of the experiment.

Fig 3. Schematic representation of *in vitro* experiment. Note that measurements taken at 4 h and 19 h are not considered in the evaluation of the amplification factor. These measurements are solely utilized to demonstrate the viability of the cells and the timescale of glucose uptake.

After sampling, the medium was frozen and kept at -80 °C until analysis. Glucose concentrations in the samples were measured using Stanbio Glucose LiquiColor test. All samples were analysed undiluted according to manufacturers instructions. In short, 5 μL sample or standard was added to a clear flat bottom 96-well plate (Nunc). The glucose reagent was pre-heated to 37 °C and the 95 μL reagent was added to start the reaction. The plate was centrifugated in short-spin to remove air bubbles and then incubated at 37 °C for 5 min. After incubation absorbance was directly measured at 520 nm on a Spectramax Plus reader and sample concentrations were calculated from the standard curve.

Results

Fig. 4 demonstrates the porosity (ϵ) and amplification factor (k) as a function of the number of cells, $15000 < N_c < 25000$ in the spheroid given a fixed radius $R_s = 226$ μm. The cell volume is assumed to be $V_c = 1.7 \times 10^{-15}$ m^3. As observed in Fig. 1, k increases exponentially with an increase in N_c. For $N_c = 25000$, which is the approximate number of cells in HepaRG spheroids, we have $\epsilon = 0.1$ and correspondingly $k = 4.49$. This value of k suggests a large concentration discontinuity at the spheroid boundary.

Fig 4. Porosity (ϵ) and concentration ratio at the boundary (k) versus the number of cells inside the spheroid (N_c).

Figs. 5(a) and 5(c) illustrate the outcomes of 8 replicates with incubation volumes of 100 μL and 75 μL. For each replicate, the glucose concentration was measured at 1, 5, and 10 min after addition of spheroids to the high-glucose medium (the raw data is provided in Supplementary Tables S2 and S3). The concentration dynamics observed in the initial 10 minutes of the PBS results indicated that utilizing the time-averaged

NGC provides a good estimate of the NGC reduction due to the spheroids. Additionally, this time-averaging approach helps to reduce the influence of the high data variability.

Fig 5. Glucose concentration measured at 1, 5, and 10 minutes after introducing the spheroid to the medium for 8 replicates of the 100 and 75 μL incubations, respectively (a,c). The 10-minute time-averages of measured concentration at 1, 5, and 10 min for each replicate and the statistical average (mean) of the replicates (shown by the purple line) (b,d).

Figs. 5(b) and 5(d) present the average of three time points at 1, 5, and 10 min (shown by green and orange bars, respectively) for each replicate and the statistical average (mean) of all replicates (shown by the purple line). The obtained average can be interpreted as the 10 min approximated average of glucose concentration. The mean glucose concentration for the 100 and 75 μL incubations is observed to be 10.67 and 10.86 M, respectively.

Fig. 6(a) illustrates the mean glucose concentration in the spheroid-free medium (based on Supplementary Table S1) and the mean time-averaged glucose concentration during the first 10 min calculated based on measurements at 1, 5, and 10 min for the 100 and 75 μL incubations. A box plot of these data is presented in Fig. 6(b), which confirms that there are no outliers based on the "median and quartiles" method.

Fig 6. (a) Mean GC in medium before adding spheroids and the mean 10 min time-averaged GC for the 100 and 75 μL incubations. (b) Boxplot of the results.

Fig. 6(a) shows that the mean glucose concentrations observed in the medium before addition of spheroids, 100 μL, and 75 μL incubations are 11.12, 10.67, and 10.86, respectively. The viability of the spheroids is evident from the reduction in glucose levels observed after 4 hours (for 100 μL) and 19 hours (for 75 μL) (provided in Supplementary Table S1 and Figure S2). Furthermore, the data shows a noticeable decrease in glucose concentration during the initial 10 minutes in both 75 and 100 μL incubations, which is more pronounced than the reduction observed after 4 hours due to glucose utilization by HepaRG cells. This finding supports the proposed theory of an amplification factor that leads to rapid glucose reduction over the timescale of initial transient diffusion. It also indicates that glucose absorption by HepaRG cells is a slow process and may not have a significant impact over this initial period. To test this hypothesis, we conducted two hypothesis tests.

The first hypothesis test compares the mean glucose concentration in the spheroid-free medium (μ_0) to the mean observed from the 100 μL experiment (μ_{100}). The null hypothesis is that the two means are equal ($\mu_0 = \mu_{100}$), while the alternative hypothesis is that the mean of the spheroid-free medium is greater than the mean of the 100 μL experiment ($\mu_0 > \mu_{100}$).

Similarly, the second hypothesis test compares the mean values for the 75 μL and spheroid-free experiment. The null hypothesis is that the mean glucose concentration in the spheroid-free medium is the same as the mean observed from the 75 μL incubation ($\mu_0 = \mu_{75}$), while the alternative hypothesis is that the mean of the spheroid-free medium is greater than the mean of the 75 μL incubation ($\mu_0 > \mu_{75}$).

As mentioned, the mean glucose concentrations observed in the medium before addition of spheroids, 100 μL, and 75 μL incubations are 11.12, 10.67, and 10.86, respectively. The corresponding variances of the data samples are 0.15, 0.05, and 0.049. Due to the differing variances in the data sets, we use a two-sample t-test assuming unequal variances. We perform a one-tailed test due to the form of the alternative hypothesis.

The resulting p-values for the first and second tests are 0.008 and 0.06, respectively. These values indicate a strongly significant difference for the first hypothesis and a marginally significant difference for the second hypothesis. Based on these results, we can conclude that the spheroids lead to a statistically significant reduction in glucose concentration during the initial 10 minutes.

In addition to the hypothesis testing, we have compared our experimental results with the glucose concentration predicted by the PBS in Fig. 7. As observed, the PBS closely follows our experimental results for both cases.

Fig 7. Experimental glucose concentration in the media compared with the predicted values obtained from the proposed PBS, assuming an initial concentration of 11.12 mM.

Conclusion

To enable the development of reliable biophysical models for 3DCAs, we utilized both theoretical and experimental methods to derive and characterize the amplification BC, which relates the concentration inside and outside the border between a 3DCA and its surrounding medium. Our biophysical theoretical analysis revealed a factor that characterizes the amplification BC and that this factor is a function of the two diffusion coefficients of the cell culture and medium. We confirmed this analytical result using a proposed PBS, which also showed a rapid decrease in the molecule concentration in the culture medium as a result of the amplification factor. To evaluate our approach, we conducted a pilot experiment using liver spheroids as the 3DCAs and glucose as the target molecule. Our study demonstrated a significant reduction in glucose concentration within the medium with $p = 0.008$ for 100 μL medium and $p = 0.06$ for 75 μL, in line with the PBS simulations.

The amplification factor revealed through our theoretical and experimental methods can have significant implications for biophysical models used in 3DCA experiments, including organ-on-a-chip models. Consideration of the amplification factor in such models would result in more accurate predictions of the biophysical models for 3DCAs, and consequently, aid in drug design and analysis of drug exposure within tissues. This factor may provide insight into the mechanisms behind tumor development and morphogenises. In particular, the packed structure of cancer tumors enables them to receive and trap a higher concentration of nutrients and oxygen molecules based on the amplification factor. Thus, this study could contribute to the development of novel approaches to manage and treat cancerous tissues. Furthermore, our study offers a generic experimental approach to quantify the amplification factor for different 3DCAs and contributes to a better understanding of this phenomenon. These types of advanced *in vitro* models will likely play a major role in future drug discovery, providing a human-cell based system that can reduce the number of animals used in research.

This was an initial pilot study using liver spheroids, and we require additional experimental data involving diverse cell types and varying conditions to more comprehensively characterize and capture the amplification property. The adoption of more precise measurement protocols and tools could prove invaluable in reducing the observed high variability.

Acknowledgments

This work was supported by the Engineering and Physical Sciences Research Council [EP/V030493/1].

References

1. Bialek W, *Biophysics: searching for principles.* Princeton University Press, 2012.
2. Bauer S, Wennberg Huldt C, Kanebratt KP, Durieux I, Gunne D, Andersson S, Ewart L, Haynes WG, Maschmeyer I, Winter A, Ämmälä C. Functional coupling of human pancreatic islets and liver spheroids on-a-chip: Towards a novel human ex vivo type 2 diabetes model. Scientific reports, 2017, 7(1), 14620.
3. Rossi G, Manfrin A, Lutolf MP. Progress and potential in organoid research. Nature Reviews Genetics, 2018, 19(11), 671-87.
4. Low LA, Mummery C, Berridge BR, Austin CP, Tagle DA. Organs-on-chips: into the next decade. Nature Reviews Drug Discovery, 2021, 20(5), 345-61.
5. Bellocchi G, Rivington M, Donatelli M, Matthews K. Validation of biophysical models: issues and methodologies. A review. Agronomy for Sustainable Development, 2010, 30(1), 109-30.
6. Tracqui P. Biophysical models of tumor growth. Reports on Progress in Physics, 2009, 72(5), 056701.
7. Jelescu IO, Palombo M, Bagnato F, Schilling KG. Challenges for biophysical modeling of microstructure. Journal of Neuroscience Methods, 2020, 344, 108861.
8. McCulloch AD. Systems biophysics: multiscale biophysical modeling of organ systems. Biophysical journal, 2016, 110(5), 1023-7.
9. Ward JP, King JR. Mathematical modelling of avascular-tumor growth. Mathematical Medicine and Biology: A Journal of the IMA, 1997, 14(1), 39-69.
10. Haass NK, Beaumont KA, Hill DS, Anfosso A, Mrass P, Munoz MA, Kinjyo I, Weninger W. Realtime cell cycle imaging during melanoma growth, invasion, and drug response. Pigment cell & melanoma research, 2014, 27(5), 764-76.
11. Crank J. *The mathematics of diffusion.* Oxford university press, 1979.
12. Astrauskas R, Ivanauskas F, Jarockyt G, Karabanovas V, Rotomskis R. Modeling the uptake of fluorescent molecules into 3D cellular spheroids. Nonlinear analysis: modelling and control, 2019, 24(5), 838-52.
13. Leedale JA, Kyffin JA, Harding AL, Colley HE, Murdoch C, Sharma P, Williams DP, Webb SD, Bearon RN. Multiscale modelling of drug transport and metabolism in liver spheroids. Interface focus, 2020, 10(2), 20190041.
14. Bull JA, Mech F, Quaiser T, Waters SL, Byrne HM. Mathematical modelling reveals cellular dynamics within tumor spheroids. PLoS computational biology, 2020, 16(8), e1007961.
15. Rousset N. Developing Modeling Approaches For Microfluidic Drop Networks. Doctoral dissertation, ETH Zurich, 2022.

16. Graff CP, Wittrup KD. Theoretical analysis of antibody targeting of tumor spheroids: importance of dosage for penetration, and affinity for retention. Cancer research, 2003, 63(6), 1288-96.

17. Goodman TT, Chen J, Matveev K, Pun SH. Spatiotemporal modeling of nanoparticle delivery to multicellular tumor spheroids. Biotechnology and bioengineering, 2008, 101(2), 388-99.

18. Grimes DR, Kelly C, Bloch K, Partridge M. A method for estimating the oxygen consumption rate in multicellular tumor spheroids. Journal of The Royal Society Interface, 2014, 11(92), 20131124.

19. Klowss JJ, Browning AP, Murphy RJ, Carr EJ, Plank MJ, Gunasingh G, Haass NK, Simpson MJ. A stochastic mathematical model of 4D tumor spheroids with real-time fluorescent cell cycle labelling. Journal of the Royal Society Interface, 2022, 19(189), 20210903.

20. Atkins, P, De Paula, J, & Keeler, J *Atkins' physical chemistry*. Oxford University Press, 2018.

21. Casas B, Vilén L, Bauer S, Kanebratt KP, Wennberg Huldt C, Magnusson L, Marx U, Andersson TB, Gennemark P, Cedersund G. Integrated experimental-computational analysis of a HepaRG liver-islet microphysiological system for human-centric diabetes research. PLOS Computational Biology, 2022, 18(10), e1010587.

22. Daunys S, Janonien A, Janukeviien I, Pakeviit M, Petrikait V. 3D tumor spheroid models for in vitro therapeutic screening of nanoparticles. Bio-Nanomedicine for Cancer Therapy, 2021, 243-70.

23. Sharifi F, Firoozabadi B, Firoozbakhsh K. Numerical investigations of hepatic spheroids metabolic reactions in a perfusion bioreactor. Frontiers in Bioengineering and Biotechnology, 2019, 7, 221.

24. Vafai K, editor. *Handbook of porous media*. Crc Press, 2015.

25. Arjmandi H, Zoofaghari M, Rezaei M, Kanebratt K, Vilen L, Janzen D, Gennemark P, Noel A. Diffusive Molecular Communication with a Spheroidal Receiver for Organ-on-Chip Systems. IEEE International Conference on Communication, Italy, Rome, May 2023.

26. Tascher, G, et al. In-depth proteome analysis highlights HepaRG cells as a versatile cell system surrogate for primary human hepatocytes. *Cells*, 8(2) (2019).

27. Rasband, W.S., ImageJ, U. S. National Institutes of Health, Bethesda, Maryland, USA, https://imagej.nih.gov/ij/, 1997-2018.

Supporting Information

Table S1 Measured glucose concentration of medium before adding the spheroids

Table S2 Measured Glucose concentration at time points 1, 5, 10 min, and 4h in 100 μL incubations.

Table S3 Measured Glucose concentration (GC) at times 1, 5, 10 min, and 19h in 75 μL incubations.

Fig S1 (a) Microscopic images of three liver spheroids at 10X magnification (scale bar is 200 μm). (b) Microscopic images of three spheroids at 4X magnification (scale bar is 200 μm).

Fig S2 Mean GC in medium before adding spheroids, mean 10 min time-averaged GC for the 100 and 75 μL incubations, mean GC at 4 hours (for 100 μL), mean GC at 19 hours (for 75 μL).

Appendix S1 Proof of Proposition 1.

Average concentration variation over time

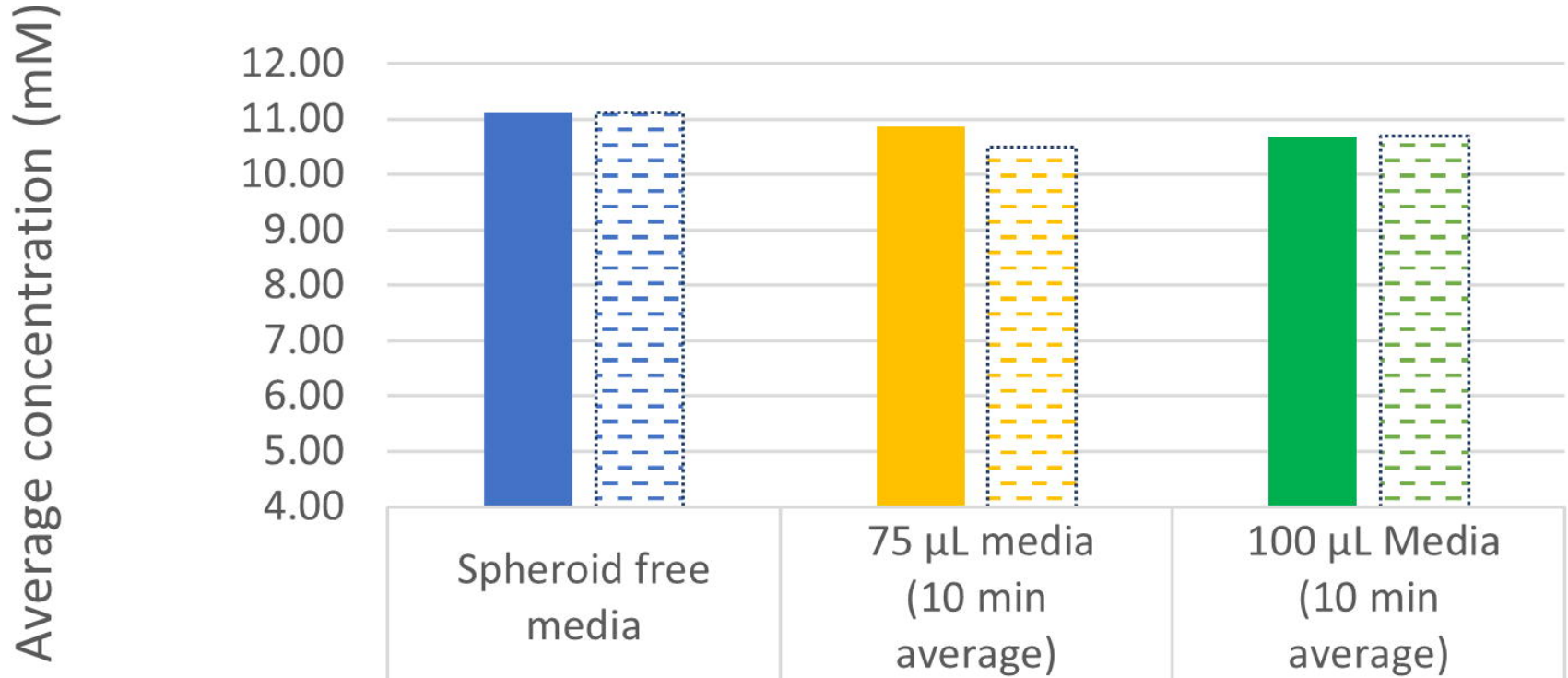

	Spheroid free media	75 µL media (10 min average)	100 µL Media (10 min average)
Experiment	11.12	10.86	10.67
Particle Based Simulator	11.12	10.48	10.69

Experiment Particle Based Simulator

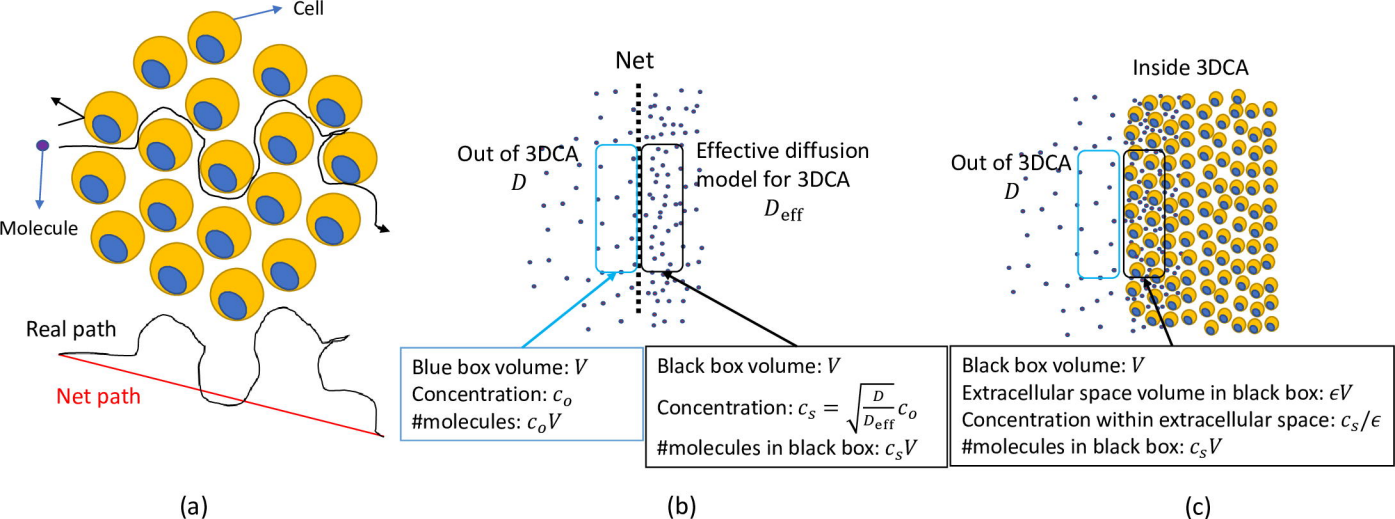
Cell
Molecule
Real path
Net path
Net
Out of 3DCA
D
Effective diffusion
model for 3DCA
D_{eff}
Inside 3DCA
Out of 3DCA
D
Blue box volume: V
Concentration: c_o
#molecules: $c_o V$
Black box volume: V
Concentration: $c_s = \sqrt{\frac{D}{D_{\text{eff}}}} c_o$
#molecules in black box: $c_s V$
Black box volume: V
Extracellular space volume in black box: ϵV
Concentration within extracellular space: c_s/ϵ
#molecules in black box: $c_s V$
(a)
(b)
(c)

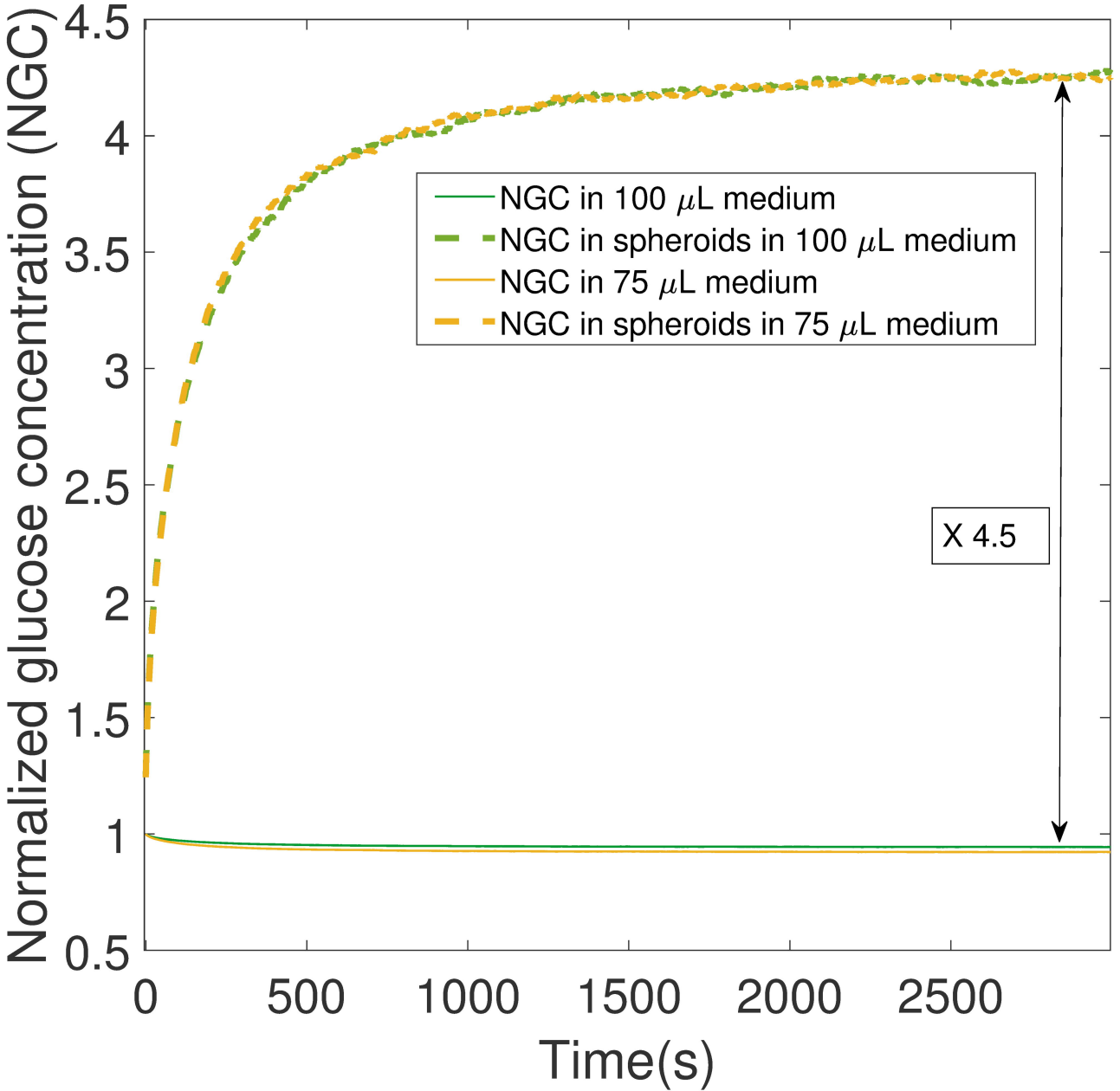
Normalized glucose concentration (NGC)
4.5
4
3.5
3
2.5
2
1.5
1
0.5
0
500
1000
1500
2000
2500
Time(s)
NGC in 100 μL medium
NGC in spheroids in 100 μL medium
NGC in 75 μL medium
NGC in spheroids in 75 μL medium
X 4.5

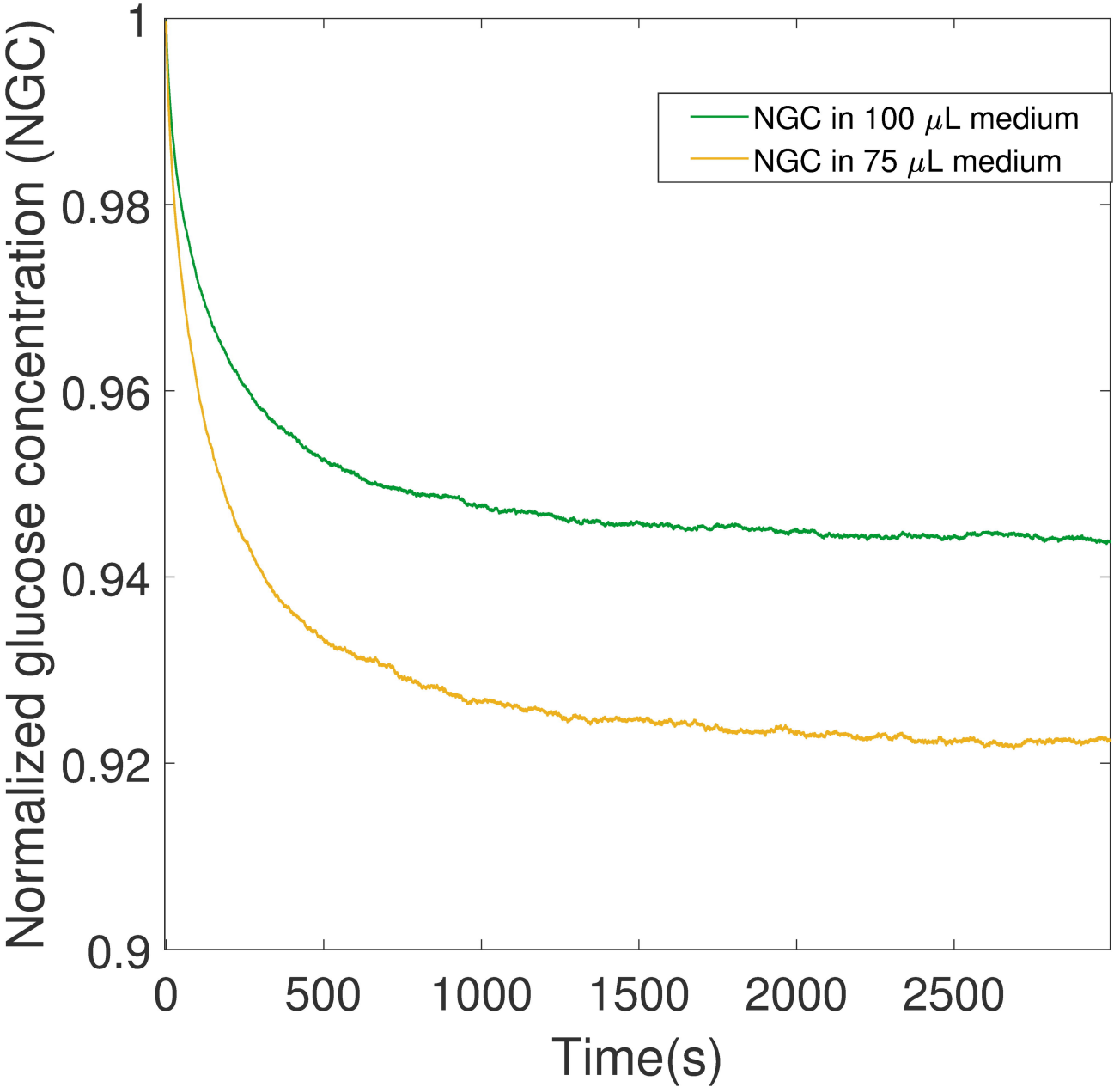
Normalized glucose concentration (NGC)
1
0.98
0.96
0.94
0.92
0.9
0
500
1000
1500
2000
2500
Time(s)
NGC in 100 μL medium
NGC in 75 μL medium

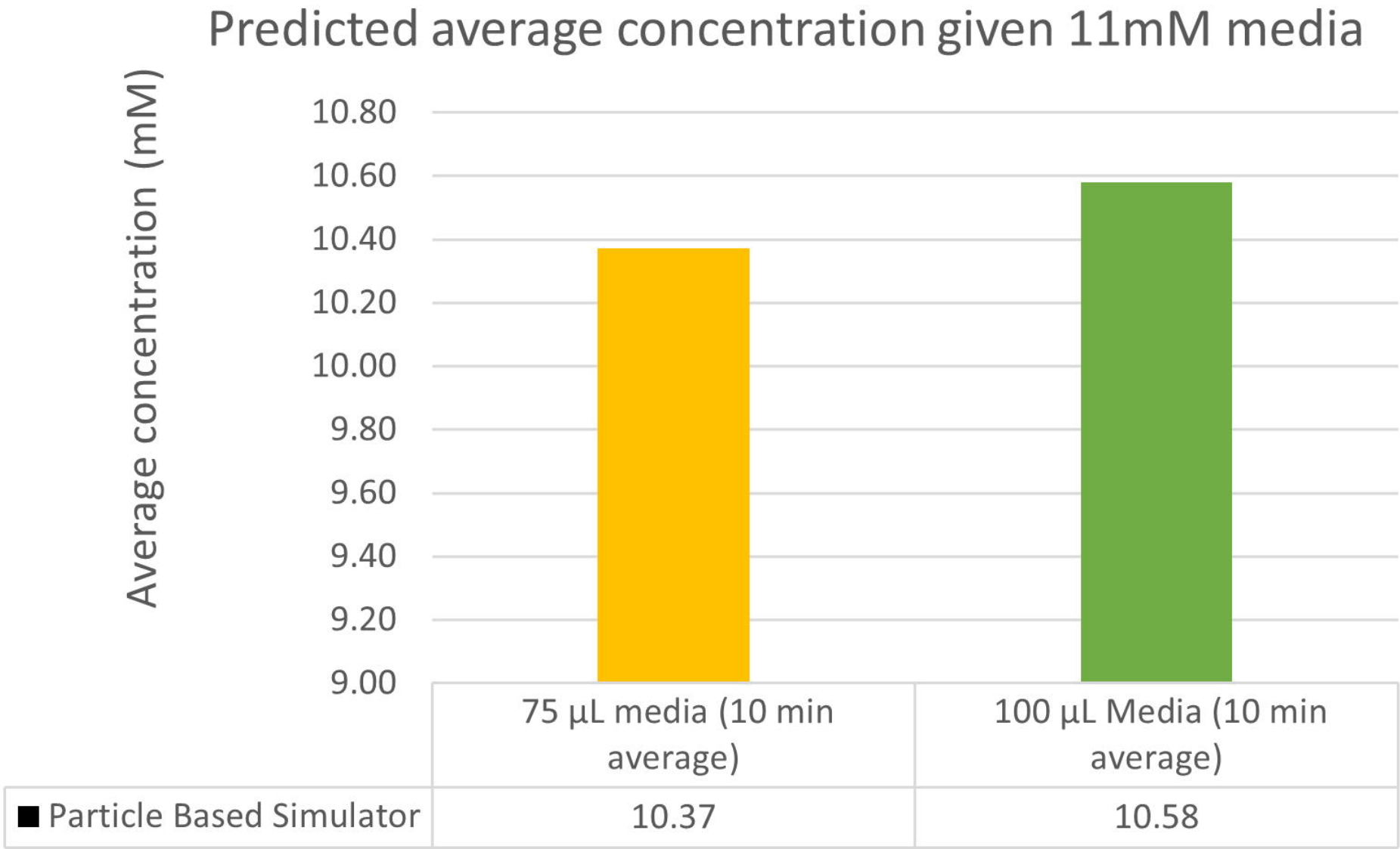
Predicted average concentration given 11mM media
Average concentration (mM)
10.80
10.60
10.40
10.20
10.00
9.80
9.60
9.40
9.20
9.00
75 µL media (10 min average)
100 µL Media (10 min average)
Particle Based Simulator
10.37
10.58

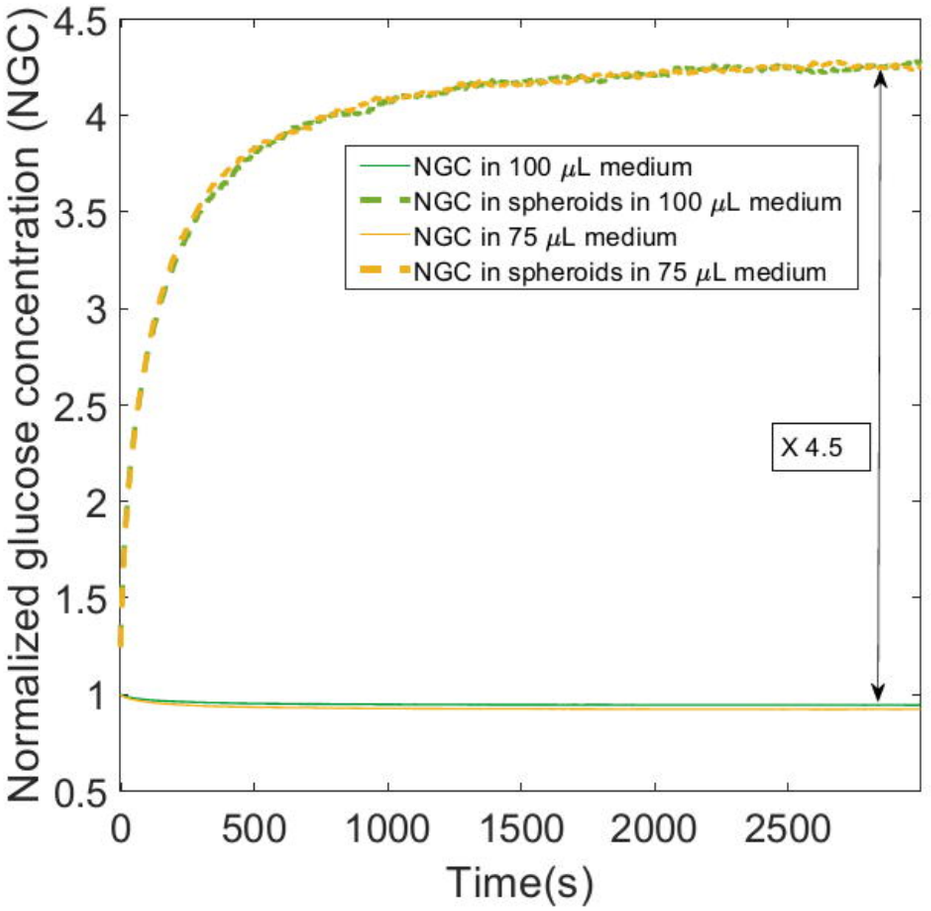
Normalized glucose concentration (NGC)
Time(s)
NGC in 100 μL medium
NGC in spheroids in 100 μL medium
NGC in 75 μL medium
NGC in spheroids in 75 μL medium
X 4.5

(a)

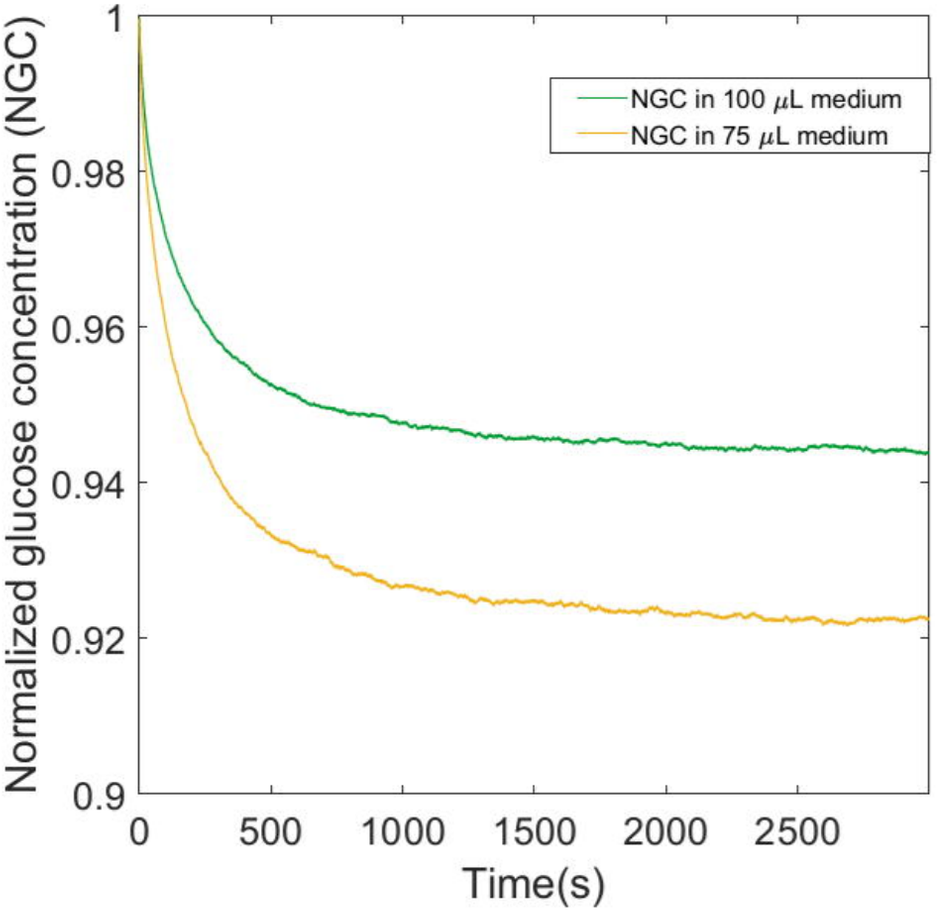
Normalized glucose concentration (NGC)
Time(s)
NGC in 100 μL medium
NGC in 75 μL medium

(b)

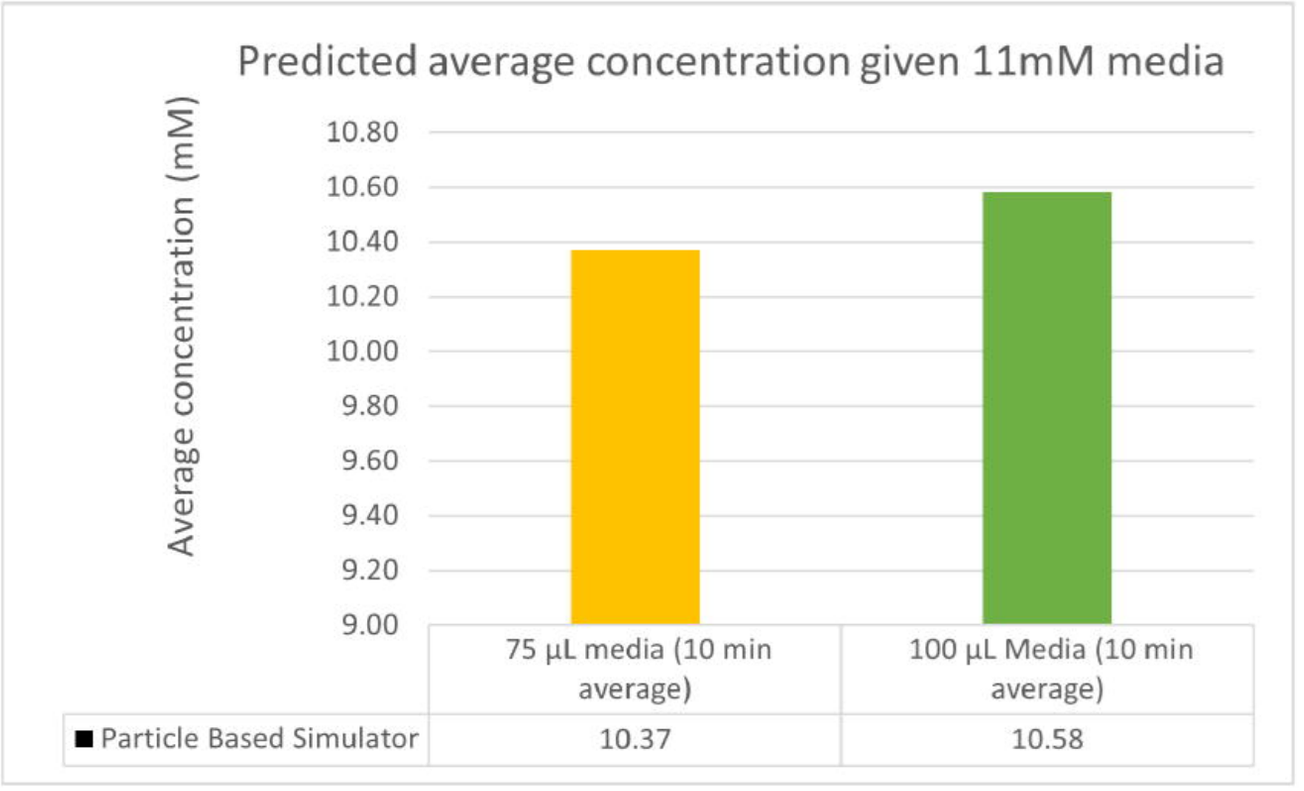
Predicted average concentration given 11mM media
Average concentration (mM)
10.80
10.60
10.40
10.20
10.00
9.80
9.60
9.40
9.20
9.00
75 μL media (10 min average)
100 μL Media (10 min average)
Particle Based Simulator
10.37
10.58

(c)

Media before adding spheroid	100 μL media with 40 spheroids	75 μL media with 40 spheroids
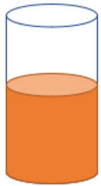	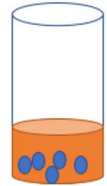	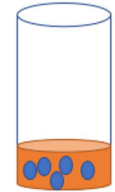
8 replicates	8 replicates	8 replicates
1 measurement at 0	4 measurements at 1 min, 5 min, 10 min, 4 h	4 measurements at 1 min, 5 min, 10 min, 19 h

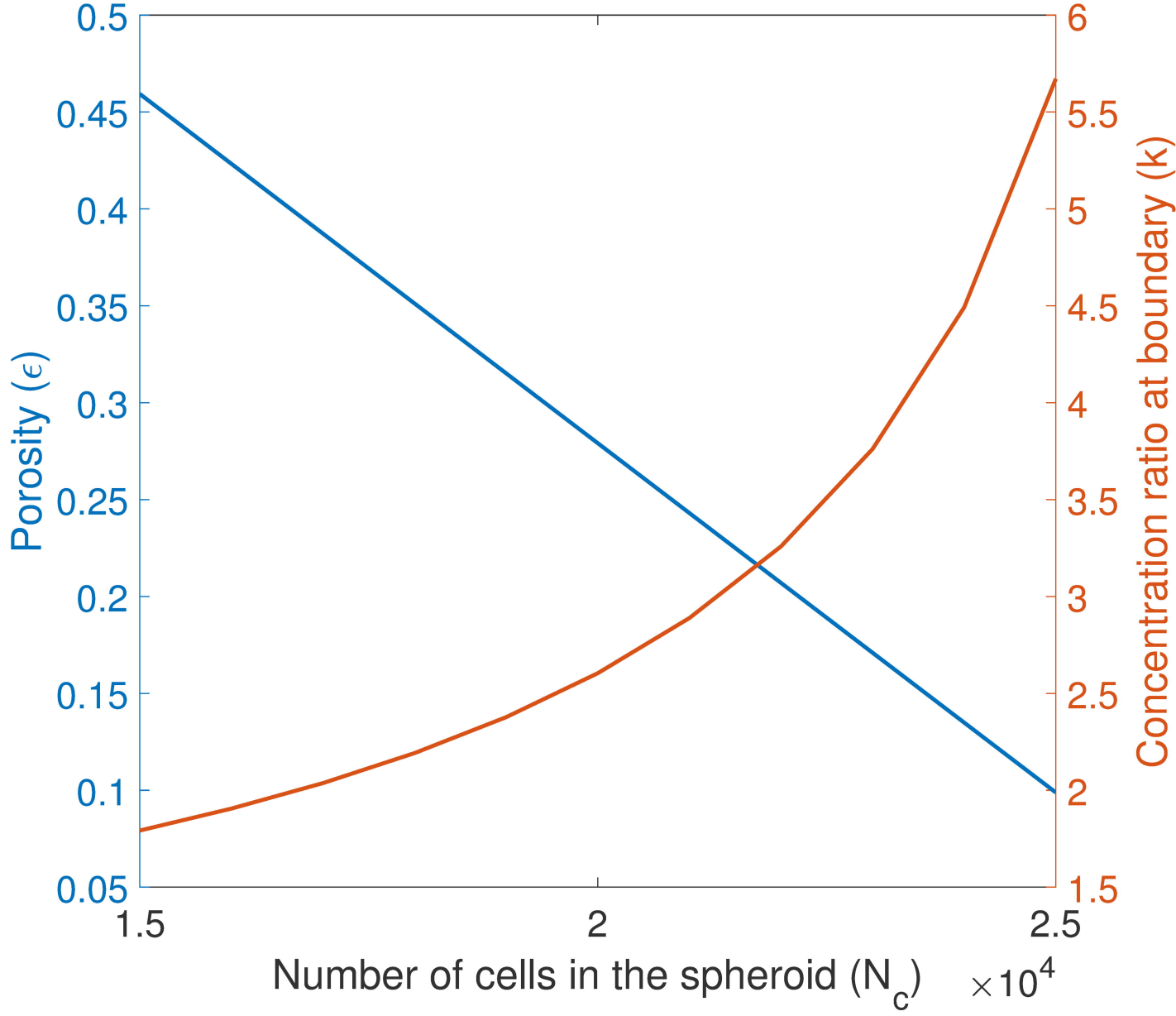
0.5
0.45
0.4
0.35
0.3
0.25
0.2
0.15
0.1
0.05
Porosity (ϵ)
6
5.5
5
4.5
4
3.5
3
2.5
2
1.5
Concentration ratio at boundary (k)
1.5
2
2.5
Number of cells in the spheroid (N_c)
×10^4

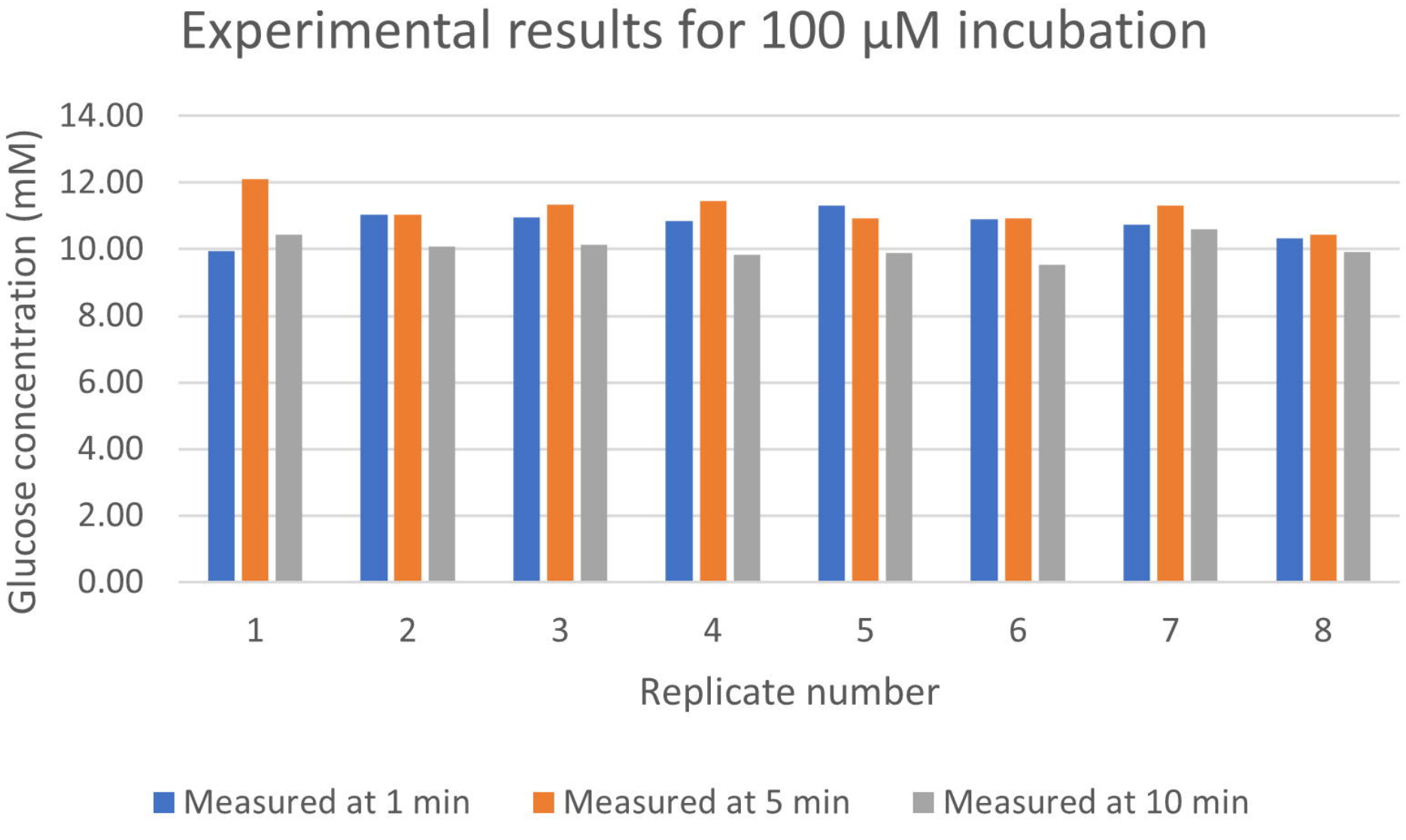
Experimental results for 100 µM incubation
Glucose concentration (mM)
14.00
12.00
10.00
8.00
6.00
4.00
2.00
0.00
1
2
3
4
5
6
7
8
Replicate number
Measured at 1 min
Measured at 5 min
Measured at 10 min

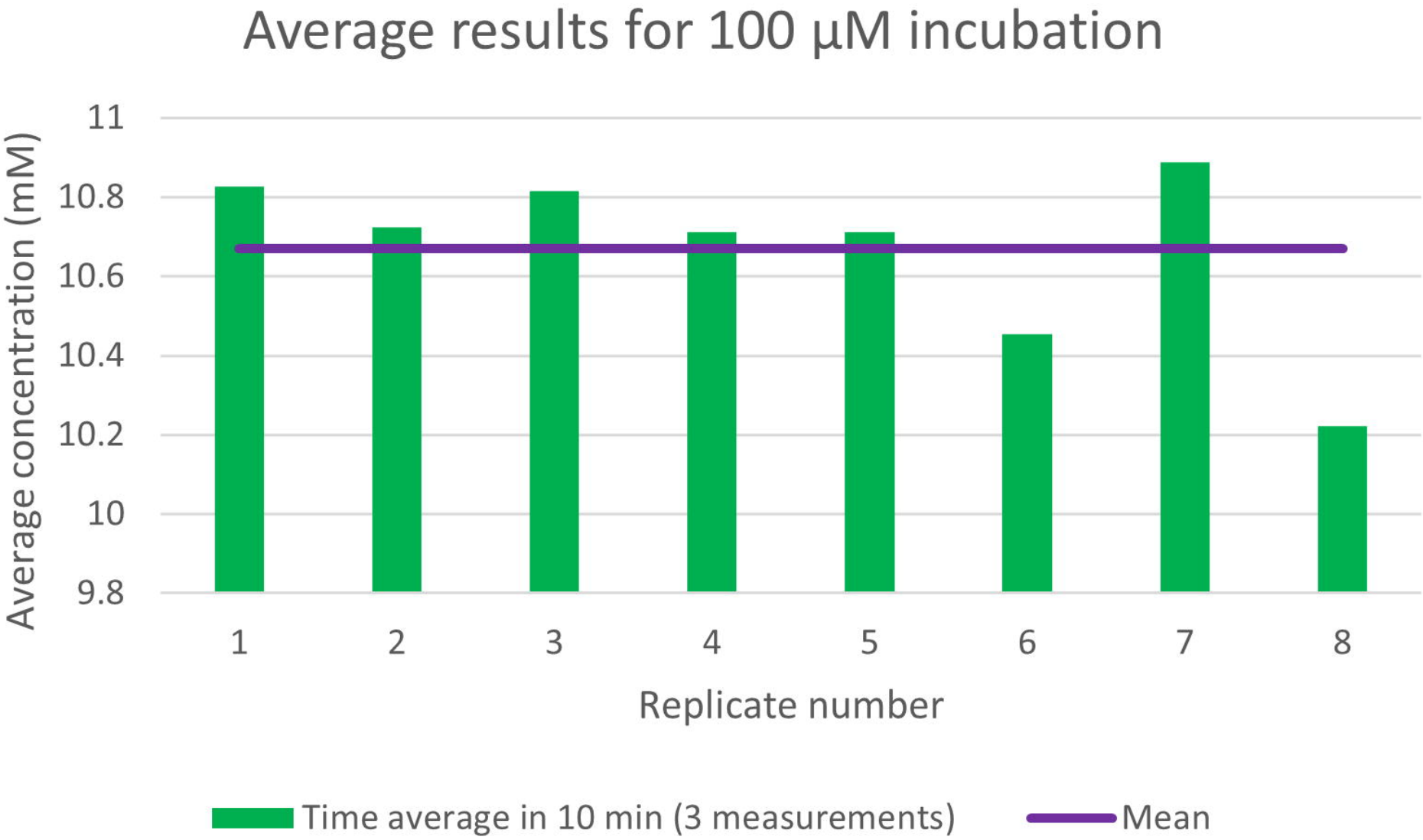
Average results for 100 µM incubation
Average concentration (mM)
11
10.8
10.6
10.4
10.2
10
9.8
1
2
3
4
5
6
7
8
Replicate number
Time average in 10 min (3 measurements)
Mean

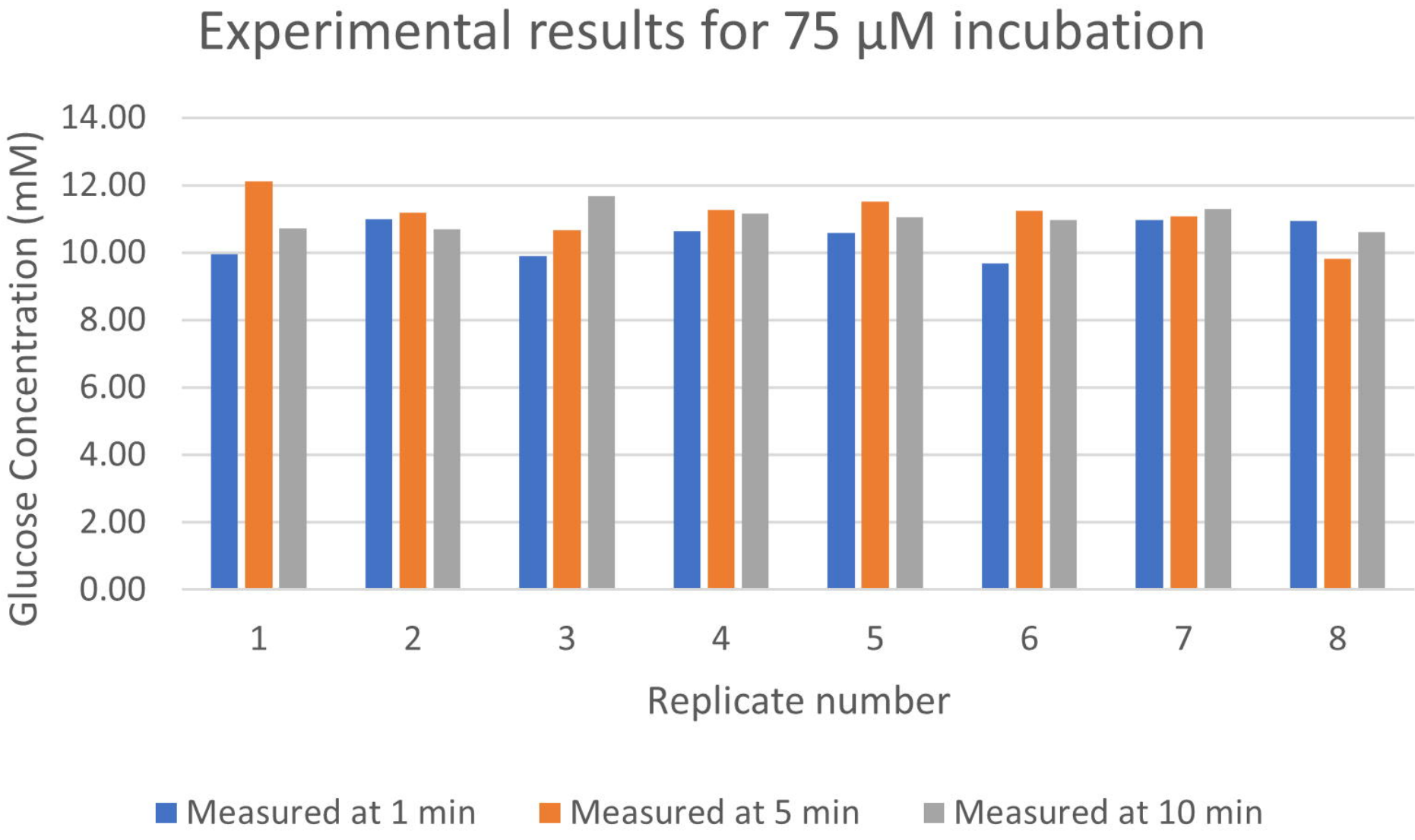
Experimental results for 75 µM incubation
Glucose Concentration (mM)
14.00
12.00
10.00
8.00
6.00
4.00
2.00
0.00
1
2
3
4
5
6
7
8
Replicate number
Measured at 1 min
Measured at 5 min
Measured at 10 min

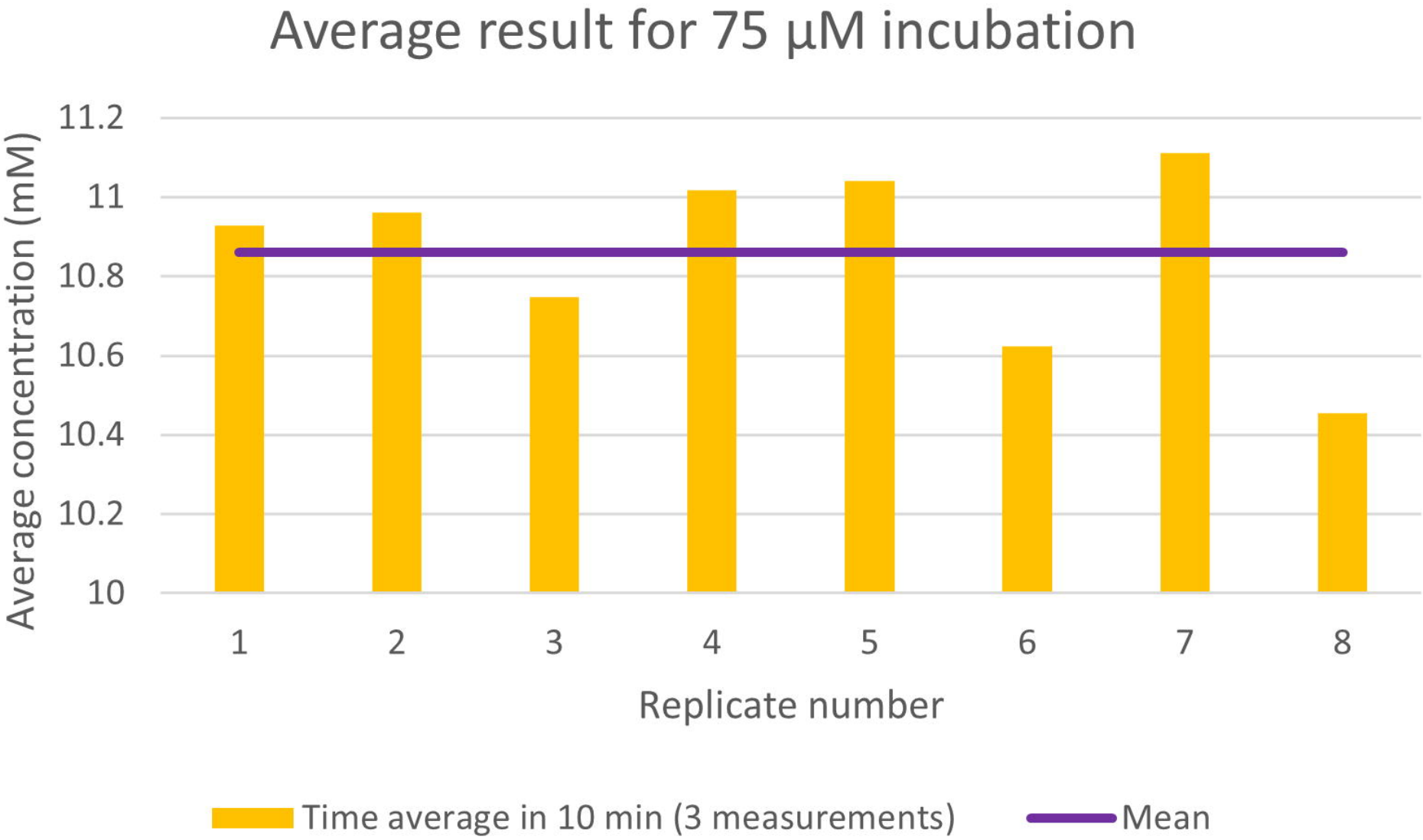
Average result for 75 µM incubation
Average concentration (mM)
11.2
11
10.8
10.6
10.4
10.2
10
1
2
3
4
5
6
7
8
Replicate number
Time average in 10 min (3 measurements)
Mean

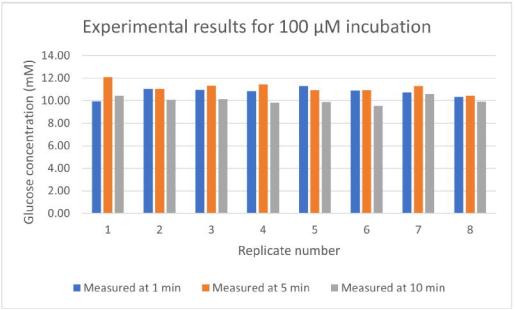
Experimental results for 100 µM incubation
Glucose concentration (mM)
14.00
12.00
10.00
8.00
6.00
4.00
2.00
0.00
1
2
3
4
5
6
7
8
Replicate number
Measured at 1 min
Measured at 5 min
Measured at 10 min

(a)

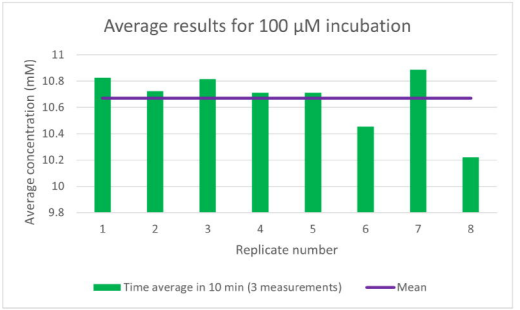
Average results for 100 µM incubation
Average concentration (mM)
11
10.8
10.6
10.4
10.2
10
9.8
1
2
3
4
5
6
7
8
Replicate number
Time average in 10 min (3 measurements)
Mean

(b)

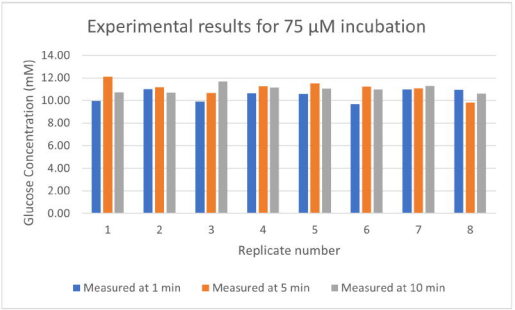
Experimental results for 75 µM incubation
Glucose Concentration (mM)
14.00
12.00
10.00
8.00
6.00
4.00
2.00
0.00
1
2
3
4
5
6
7
8
Replicate number
Measured at 1 min
Measured at 5 min
Measured at 10 min

(c)

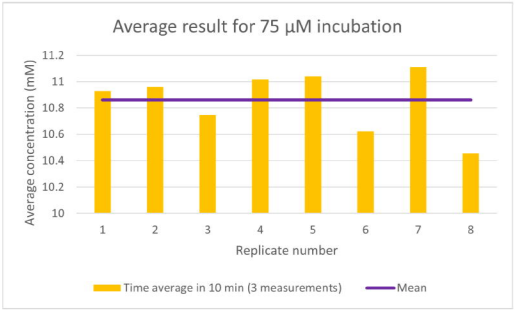
Average result for 75 µM incubation
Average concentration (mM)
11.2
11
10.8
10.6
10.4
10.2
10
1
2
3
4
5
6
7
8
Replicate number
Time average in 10 min (3 measurements)
Mean

(d)

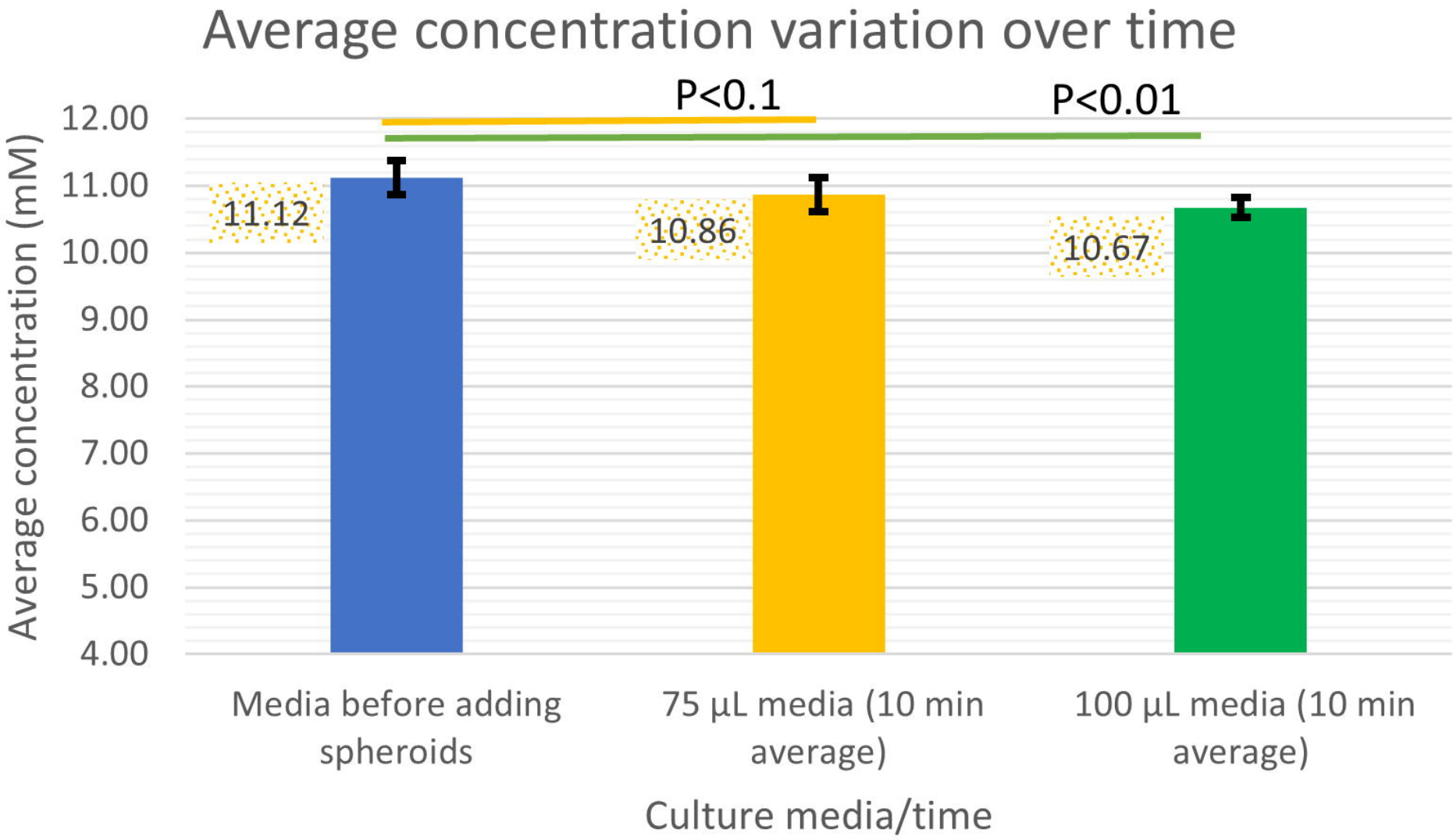
Average concentration variation over time
P<0.1
P<0.01
12.00
11.00
10.00
9.00
8.00
7.00
6.00
5.00
4.00
Average concentration (mM)
11.12
10.86
10.67
Media before adding spheroids
75 µL media (10 min average)
100 µL media (10 min average)
Culture media/time

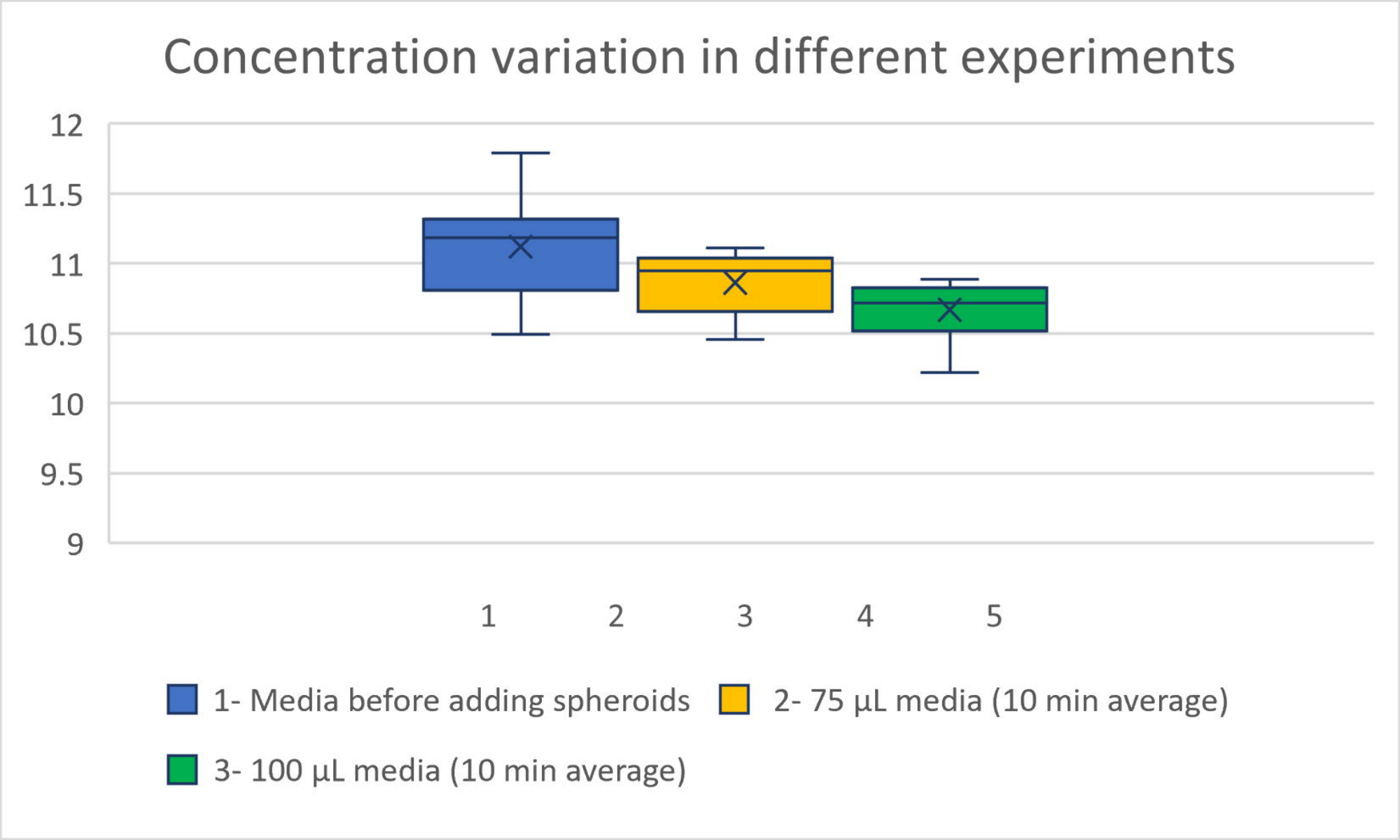
Concentration variation in different experiments
12
11.5
11
10.5
10
9.5
9
1
2
3
4
5
1- Media before adding spheroids
2- 75 µL media (10 min average)
3- 100 µL media (10 min average)

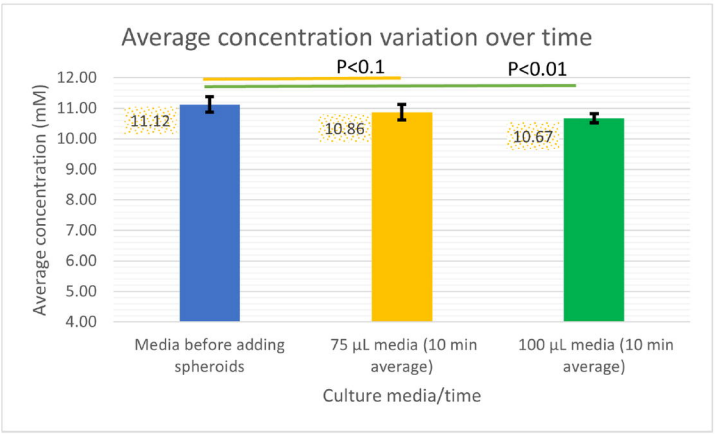
Average concentration variation over time
P<0.1
P<0.01
11.12
10.86
10.67
Average concentration (mM)
12.00
11.00
10.00
9.00
8.00
7.00
6.00
5.00
4.00
Media before adding spheroids
75 µL media (10 min average)
100 µL media (10 min average)
Culture media/time

(a)

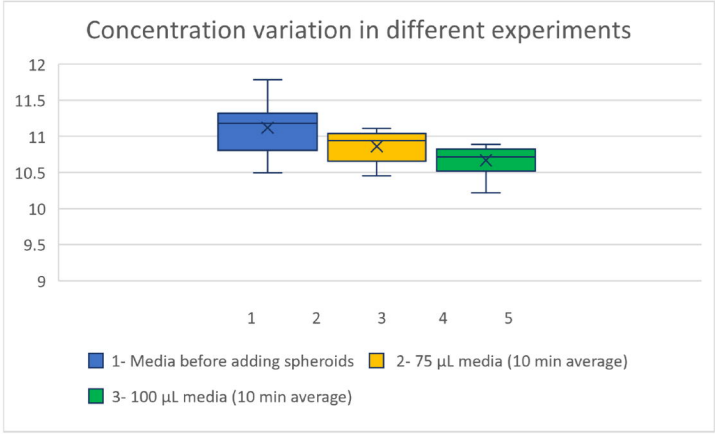
Concentration variation in different experiments
12
11.5
11
10.5
10
9.5
9
1
2
3
4
5
1- Media before adding spheroids
2- 75 µL media (10 min average)
3- 100 µL media (10 min average)

(b)